Wulf, S., Dräger, N., Ott, F., Serb, J., Appelt, O., Guðmundsdóttir, E., van den Bogaard, C., Słowiński, M., Błaszkiewicz, M., Brauer, A. (2016): Holocene tephrostratigraphy of varved sediment records from Lakes Tiefer See (NE Germany) and Czechowskie (N Poland). - *Quaternary Science Reviews*, *132*, pp. 1—14

DOI: http://doi.org/10.1016/j.quascirev.2015.11.007

Holocene tephrostratigraphy of varved sediment records from Lakes Tiefer See (NE Germany) and Czechowskie (N Poland)

Sabine Wulf [1,2*], Nadine Dräger [1], Florian Ott [1], Johanna Serb [1], Oona Appelt [3], Esther Guðmundsdóttir [4], Christel van den Bogaard [5], Michał Słowiński [6], Mirosław Błaszkiewicz [6], Achim Brauer [1]

[1] GFZ German Research Centre for Geosciences, Section 5.2 - Climate Dynamics and Landscape Evolution, Telegrafenberg, D-14473 Potsdam, Germany

[2] Senckenberg Research Institute and Natural History Museum, BIK-F, TSP6 Evolution and Climate, Senckenberganlage 25, D-60325 Frankfurt a.M., Germany

[3] GFZ German Research Centre for Geosciences, Section 3.3 - Chemistry and Physics of Earth Materials, Telegrafenberg, D-14473 Potsdam, Germany

[4] Faculty of Earth Sciences, Institute of Earth Sciences, University of Iceland, Strulugata 7, 101 Reykjavík, Iceland

[5] Helmholtz Centre for Ocean Research Kiel, GEOMAR, Wischhofstrasse 1-3, D-24148 Kiel, Germany

[6] Polish Academy of Sciences, Institute of Geography and Spatial Organization, Department of Environmental Resources and Geohazards, Kopernika 19, Torun 87-100, Poland

* Corresponding author: Sabine.Wulf@senckenberg.de (S. Wulf), Facsimile: +49-(0)6221-545503

Abstract

A detailed Holocene tephrostratigraphic framework has been developed for two predominately varved lake sediment sequences from NE Germany (Lake Tiefer See) and central N Poland (Lake Czechowskie). A total of thirteen tephras and cryptotephras of Icelandic provenance were detected and chemically fingerprinted in order to define

correlatives and to integrate known tephra ages into the sediment chronologies. Out of these, three cryptotephras (Askja-AD1875, Askja-S and Hässeldalen) were identified in both records, thus allowing a detailed synchronization of developing high-resolution palaeoenvironmental proxy data. The early Holocene Saksunarvatn Ash layer and the middle Holocene Lairg-B and Hekla-4 cryptotephras in Lake Tiefer See are further important anchor points for the comparison with other high-resolution palaeoclimate records in Central and Northern Europe. Tentative correlations of cryptotephras have been made with a historical basaltic Grimsvötn eruption (~ AD890 - AD856) and three late Holocene rhyolitic eruptions, including the 2.1 ka Glen Garry and two unknown high-silicic cryptotephras of probably Icelandic provenance (~ 1.9 cal ka BP).

1. Introduction

In the light of global warming and possibly related socio-environmental responses it is essential to understand the mechanism and timing of abrupt climate changes. Past climate variability can be best reconstructed by studying high-resolution geological records, e.g. annually laminated (varved) lake sediments. However, such records are rare in northern central Europe and are restricted to either the Lateglacial (e.g. Brauer et al., 1999; Goslar et al., 1999; Goslar et al., 1993; Merkt and Müller, 1999; Neugebauer et al., 2012) or the Holocene epoch (e.g. Dörfler et al., 2012; Enters et al., 2010; Zolitschka, 1990).

The Virtual Institute for Integrated Climate and Landscape Evolution Analyses ICLEA (www.iclea.de) aims at the continuous and high-resolution reconstruction of past climate variability and environmental changes in the northern central European Lowlands since the end of the last Ice Age. A current focus is set on two predominately varved sediment sequences from NE Germany (Lake Tiefer See; Dräger et al., 2014) and central N Poland (Lake Czechowskie; Ott et al., 2014). A high-resolution palaeoenvironmental reconstruction and the establishment of independent chronologies of both records is in progress and will enable the determination of effects of spatial and temporal climatic changes due to the existing gradient of increasing climatic continentality from the western (Tiefer See) towards the eastern archive (Czechowskie). Independent chronologies will be achieved by varve counting, radiometric dating and tephrochronology. The latter method involves the use of tephra layers (volcanic fallout material) in sedimentary repositories as a dating and synchronization tool (e.g. Lowe, 2011). Several distinct tephras of Icelandic and Eifel provenance have been reported from sites in NE Germany and western Poland, i.e. the Saksunarvatn Ash (Bramham-Law et al., 2013), the Askja-S, Hässeldalen and Laacher See tephras (e.g. Housley et al., 2013a; Juvigné et al., 1995; Lane et al., 2011b; Riede et al., 2011; Wulf et al., 2013). Those tephras, however, are restricted to the Lateglacial and early Holocene epoch. The identification of younger tephras is so far limited to a single finding of the late Holocene Glen Garry cryptotephra (non-visible tephra) in an archaeological site in NW Poland (Housley et al., 2013b).

In this study, we present a comprehensive tephrostratigraphy for the northern central European Lowlands for the last ca 11,500 years, constrained from the ICLEA sites Lake Tiefer See and Lake Czechowskie. The tephra results are used to construct robust tephrochronologies for both records in order to support their varve chronologies. They furthermore provide important anchor points for the synchronization of palaeo-proxy data of these records with each other and with other high-resolution terrestrial records in northern-central Europe.

2. Study area

Lake Tiefer See (TSK = Tiefer See Klocksin) and Lake Czechowskie (JC = Jezioro Czechowskie) are both located in the northern central European Lowlands in the foreland of the terminal moraine of the Pomeranian ice advance of the last glaciation, which is dated at 15.6 ± 0.6 ^{10}Be ka (Rinterknecht et al., 2014) (Fig. 1). Both lakes have a melt genesis, namely lake basins formed by the melting of buried ice blocks (Błaszkiewicz et al., 2011, 2015; Kaiser et al., 2012; Loon et al., 2012; Słowiński, 2010; Słowiński et al., in press). Lake Tiefer See is a 1.6 km N-S elongated lake located in the natural park of Nossentiner-Schwinzer Heide, NE Germany (53°35.5'N, 12°31.8'E, 62 m a.s.l.). It is part of the Klocksin Lake Chain that formed in a subglacial gully system during the last deglaciation. The lake has a surface area of 0.75 km^2 and a maximum water depth of 62.5 m (Dräger et al., 2014; Kienel et al., 2013).

Lake Czechowskie is situated in the eastern part of the Pomeranian Lakeland in the Tuchola Pinewoods, central N Poland (53°52.2'N, 18°14.1'E, 108 m a.s.l.). The current lake together with the adjacent Trzechowskie palaeolake (TRZ) basin (53°52.4'N, 18°12.9'E, 111 m a.s.l.) developed in a subglacial channel in the outwash plain of the Wda river, which was accumulated during the retreat of the Late Weichselian ice sheet recession between 17 and 16 cal ka BP (Błaszkiewicz et al., 2015; Marks, 2012). Lake Czechowskie has an oval-shaped basin with a surface area of 0.73 km^2 and a maximum water depth of 32 m (Błaszkiewicz, 2005; Ott et al., 2014).

Lake Tiefer See and Lake Czechowskie are both located in a distal position to Icelandic volcanoes (2,150 – 2,400 km SE) and the W German Eifel Volcanic Field (500 – 840 km NE).

3. Methods

3.1 Sediments and developing chronology

3.1.1 Lake Tiefer See

In the years 2011 and 2013, a total of seven parallel sediment sequences and several surface cores were recovered from the deepest part of Lake Tiefer See using an UWITEC piston corer (Fig. 1b). These sequences were used to construct a composite profile of 1083 cm length that reaches the basal glacio-fluvial sand deposits (Fig. 2a). Two sediment gaps probably of several decimetres each occur at 769.5 cm and 956.5 cm depth as a result of technical problems during coring. The chronology of the composite profile is under construction and will incorporate several dating methods, i.e. varve counting, estimation of sedimentation rates in poorly and non-varved sections, AMS-^{14}C dating (Dräger et al., 2014) and tephrochronology (this paper). Lacustrine sediments are characterized by alternating finely laminated and homogenous diatomaceous gyttia with various amounts of calcareous and detrital matter (Dräger et al., 2014; Kienel et al., 2013).

3.1.2 Lake Czechowskie

Four parallel and overlapping sediment sequences as well as numerous short cores were retrieved between 2009 and 2012 from the deepest parts of Lake Czechowskie (Fig. 1b) using an UWITEC piston corer and a Ghilardi Gravity Corer (KGH 94), respectively. A continuous composite profile of 1346 cm length has been constructed (Fig. 2b) by defining unambiguous correlation layers. Holocene sediments are dominated by finely laminated calcareous gyttia with various amounts of organic and detrital matter. The base of Lateglacial sedimentary deposits is characterised by coarse glacio-fluvial sand deposits (Ott et al., 2014). Dating of sediments is in progress and will include varve counting, AMS ^{14}C dating, radionuclide distribution (^{137}Cs) (Ott et al., 2014) and tephrochronology (this paper).

3.2 Tephrochronological methods

A systematic scanning for cryptotephras in TSK and JC sediments was carried out using preliminary chronostratigraphical information, high-resolution sampling and processing of sediments for each archive. Continuous sediment samples of 1 cm^3 were taken in 0.5 cm to 5 cm intervals for the entire Holocene TSK sequence as well as for the early Holocene part of JC sediments. A selective search in the middle to late Holocene section of the JC sequence was carried out depending on tephra findings in this time interval in the TSK sequence. In order to remove organic matter, samples were individually treated with a 15% hydrogen peroxide (H_2O_2) solution (overnight) and subsequently wet-sieved over a 100-µm and 20-µm mesh sieve. In the following, a 10% hydrochloric acid (HCl) solution was added to the 20-100 µm fractions in order to dissolve calcium carbonates (maximum 1 hour). The residual samples were then repeatedly rinsed with deionized water and dried with Ethanol at 60°C. Samples with high diatom abundances were additionally heated in a 2M sodium carbonate (Na_2CO_3) solution in a water bath for 5 hour, neutralized with a 10% hydrochloric acid solution and rinsed with deionized water before drying. Dried samples were inspected for volcanic glass shards on plastic lids using a transmitted light microscope (Zeiss Jenapol). Identified shards were handpicked into a single-hole-stub, embedded in Araldite 2020 resin, sectioned and polished by hand on wet silicon carbide paper.

The major element composition of single glass shards was obtained on the carbon-coated stubs at a JEOL JXA-8230 microprobe at the German Research Centre for Geosciences (GFZ). Operating conditions used a 15 kV voltage, a 10 nA beam current and beam sizes of 5 µm, 8 µm or 10 µm. Exposure times for each analysis were 20 seconds for the elements Fe, Cl, Mn, Ti, Mg and P, as well as 10 seconds for F, Si, Al, K, Ca and Na. Instrumental calibration used natural mineral and the Lipari obsidian glass standards (Hunt and Hill, 1996; Kuehn et al., 2011). Raw values of glass data are provided in Tables 1 and 2. For comparison, several Holocene Icelandic tephras were analysed with the same instrument, i.e. Askja-AD1875 (sample provided by C. van den Bogaard), Landnám-AD870, Eldgjá-AD~934, Hekla-3 and Hekla-4 (see Supplementary File 1). Geochemical bi-plots used normalized (water-free) data of the TSK, JC and proximal tephra samples for the comparison with other published EPMA glass data (Fig. 4).

4. Results and discussions

Tephras from both records are described from the oldest to the youngest deposition. If not indicated otherwise, the number of counted glass shards is related to 1 cm^3 of the original wet sediment sample. Tephras are labelled according to their position in the individual core sections (for example: Tephra in Lake Tiefer See, core K3, between 42 and 43 cm core depth = TSK_K3_42-43_T). The position of cryptotephras in the core section was defined as the mid-point sample depth.

A total of eight (TSK) and five (JC) cryptotephras have been identified, respectively (Tables 1, 2; Fig. 2). The tephras all show either rhyolitic (n=11) or basaltic (n=2) compositions typical of Icelandic provenance. Three samples, namely TSK11_A3_120-125_T, TSK13-F6_91-92_T and JC12_D6_112-113_T, were analysed with a small beam size of 5 µm due of the small grain sizes and high vesicularity of glass shards. Those analyses have been affected by sodium migration, resulting in slightly higher SiO_2 and lower Al_2O_3 and Na_2O concentrations (see data of Lipari standard for comparison; Supplementary File 1). However, all elemental data of those samples fully plot within the chemical fields of published glass data of potential tephra correlatives and thus enabled reliable attributions (Fig. 4).

4.1 Lake Tiefer See Holocene tephrostratigraphy

Sample TSK13_F6_99-100_T (Hässeldalen)

The lowermost cryptotephra TSK13_F6_99-100_T in Lake Tiefer See occurs in 1031.7 cm composite depth in a non-varved interval and reveals only 2 shards cm^{-3}. No further glass shards have been detected in the overlying and underlying sediments, suggesting an undisturbed and primary deposition of this cryptotephra. Both colourless, highly vesicular glass shards (Fig. 3) show rhyolitic compositions that are best comparable with those of the early Holocene Hässeldalen tephra (HDT) from the Snæfellsjökull volcano (?) in W Iceland (Davies et al., 2003) (Fig. 4f). The HDT was first reported at the distal Hässeldala port palaeolake site in southern Sweden and dated by Bayesian ^{14}C modelling at 11,380 ± 216 cal yr BP (Davies et al., 2003; Wohlfarth et al., 2006). Further findings include sites in SW Sweden (Lilja et al., 2013), Denmark (Larsen and Noe-Nygaard, 2014) and on the Faroe Islands (Lind and Wastegård, 2011). The occurrence of the HDT in TSK is in agreement with recent findings at Endinger Bruch in NE Germany (Lane et al., 2011b) and at the Węgliny site in SW Poland (Housley et al., 2013a) (Fig. 5).

Sample TSK13_F6_91-92_T (Askja-S)

Sample TSK13_F6_91-92_T in 1023.2 cm composite depth exhibited 3 shards cm^{-3} (Fig. 3) that occurs within a non-laminated section 7 cm above the Hässeldalen Tephra. Glass shards are colourless, highly vesicular and display a homogenous Icelandic rhyolitic composition with relatively low potassium values of ca 2.5 wt% and high CaO concentrations (ca 1.6-1.7 wt%) (Fig. 4f). Both the glass chemistry and the position of cryptotephra TSK13_F6_91-92_T above the biostratigraphically defined Younger Dryas/Holocene transition confirm an origin from the Askja-S caldera forming eruption of the Dyngjufjöll volcanic centre in north-eastern Iceland (Sigvaldason, 2002). The Askja-S tephra has been so far identified in lake and peat sequences on the Faroe Islands (Lind and Wastegård, 2011), in N Ireland (Turney et al., 2006), S Sweden (Davies et al., 2003; Lilja et al., 2013), NE Germany (Lane et al., 2011b) and Switzerland (Lane et al., 2011a) (Fig. 5). Its age is constrained by Bayesian ^{14}C modelling at the Hässeldala port palaeolake site in SE Sweden at 10,810 ± 240 cal yr BP (Wohlfarth et al., 2006) and in Lake Soppensee at 10,846 ± 145 cal yr BP (Lane et al., 2011a). An age estimate from Faroe Island provided a much younger time constraint at 10,350-10,500 cal yr BP (Lind and Wastegård, 2011). Ages from Hässeldala port and Soppensee were incorporated into a new age model by Bronk Ramsey et al. (2015) providing the most recent age estimate of the Askja-S tephra at 10,830 ± 57 cal yr BP.

Sample TSK13_F6_55_T (Saksunarvatn)

In 989.2 cm composite depth a 0.3 mm thick, macroscopic visible tephra layer occurs directly below a varved interval, here labelled as sample TSK13_F6_55_T. Volcanic glass shards (>100 shards cm^{-3}) of this tephra are brownish, show a low vesicularity (Fig. 3), and display a basaltic composition. The stratigraphic position in faintly laminated TSK sediments indicates a deposition during the Early Holocene (Fig. 2). Both the geochemical and chronostratigraphical data confirm a correlation with the Saksunarvatn Ash (SA) from the Grimsvötn volcanic system (Fig. 4e). The Saksunarvatn Ash is an important isochron in environmental records in northern Europe (e.g. Aarnes et al., 2012; Birks et al., 1996; Bramham-Law et al., 2013; Jóhansen, 1985; Lind and Wastegård, 2011; Lind et al., 2013; Mangerud et al., 1986; Merkt et al., 1993), the North Atlantic region (e.g. Andrews et al., 2002; Haflidason et al., 1990; Jóhannesdóttir et al., 2005; Kylander et al., 2011; Jennings et al., 2014) and Greenland (e.g. Abbott and Davies, 2012; Grönvold et al., 1995; Mortensen et al., 2005; Zielinski et al., 1997). At least two distinct SA plumes/eruptions are proposed (e.g. Jóhannesdóttir et al., 2005; Davies et al., 2012; Bramham-Law et al., 2013): one is distributed towards the SE and radiocarbon dated in Lake Kråkenes, Norway, at 10,210 ± 35 cal yr BP (Lohne et al., 2013) and another one towards the NW revealing an slightly older age but overlapping within the 2σ error range at 10,297 ± 45 cal yr BP (10,347 ± 45 yr b2k; Rasmussen et al., 2006) in the Greenland ice core record. The Saksunarvatn Ash in Lake Tiefer See is most likely related to the south-easterly dispersal fan (Fig. 5) at 10,210 ± 35 cal yr BP. Since this tephra occurs right below a laminated section (Fig. 2), it represents an important time and correlation marker in TSK sediments (Fig. 6).

Sample TSK13_F5_37-43_T (Lairg B)

Cryptotephra TSK13_F5_37-43_T occurs in 791.5 cm composite depth and is represented by the finding of two glass shards in a 5-cm^3 sediment sample obtained from varved sediments ca 22 cm below the upper sediment gap (Fig. 2). Glass shards are colourless, highly vesicular and show a rhyolitic composition, which strongly resembles the glass composition of early Holocene tephras from the Torfajökull volcanic system in southern Iceland. The best chemical match is given for the Lairg-B and Høvdarhagi tephras (Fig. 4d). Lairg-B has been identified in sites in Scotland (Dugmore et al., 1995b; Pilcher et al., 1996), Ireland (Chambers et al., 2004) and N Germany (van den Bogaard and Schmincke, 2002; Dörfler et al., 2012) and is radiocarbon dated at 6,675 ± 49 cal yr BP (Pilcher et al., 1996) and 6,723 ± 108 cal yr BP (Dörfler et al., 2012), respectively. The Høvdarhagi tephra is only known from Faroe Islands lake sediment sequences, where it is dated at 9,850-9,600 cal yr BP (Lind and Wastegård, 2011) and thus only few hundred years younger than the Saksunarvatn Ash. Cryptotephra TSK13_F5_37-43_T, however, is positioned ca. 2 m above the Saksunarvatn Ash in TSK sediments and preliminary varve counts and sedimentation rate estimates indicate a few thousand years younger age in the range of the Lairg-B tephra. In addition to the finding of Lairg-B in the nearby Lake Belauer See (Dörfler et al., 2012), this is a major criterion for a preferred correlation of cryptotephra TSK13_F5_37-43_T with Lairg-B. Despite the low number of detected glass shards and the relatively broadly defined position within a 5-cm sediment interval (higher resolution sampling revealed no further shard findings), the Lairg-B tephra is considered to provide an anchor point at a weighted mean age of 6,683 ± 45 cal yr BP (calculated after Froggatt and Lowe, 1990) for the floating TSK varve chronology (Figs. 2, 6).

Sample TSK11_A3_120-125_T (Hekla-4)

Cryptotephra TSK11_A3_120-125_T occurs at 607.9 cm composite depth and revealed two colourless, highly vesicular glass shards in a 5-cm^3 sample. The rhyolitic composition of both shards is almost identical and resembles the glass composition of distal middle to late Holocene tephras from Hekla volcano (e.g. Larsen and Thorarinsson, 1977; Sverrisdottir, 2007) (Fig. 4d). At least five widespread and geochemically similar tephras occurred during this time from Hekla, i.e. Hekla-3 (3.0 cal ka BP), Hekla-S/Kebister (3.8 cal ka BP), Hekla-4 (4.3 cal ka BP), Lairg-A (6.95 cal ka BP) and Hekla-5 (7.1 cal ka BP) (e.g. Dugmore et al., 1995a; Óladóttir et al., 2011; Guðmundsdóttir et al., 2011). All these tephras are confirmed in sites in N central Germany (van den Bogaard et al., 2002; van den Bogaard and Schmincke, 2002; Dörfler et al., 2012) (Fig. 5). The best geochemical and chronostratigraphical match of the TSK tephra is achieved with the Hekla-4 tephra (Fig. 4c). The age of the Hekla-4 tephra is constrained by radiocarbon dating at 4,218 ± 65 cal yr BP (Dugmore et al., 1995a) and 4,260 ± 20 cal yr BP (Pilcher et al., 1995), and by varve counting in Lake Belauer See and Swedish sites at 4,342 ± 75 cal yr BP (Dörfler et al., 2012) and 4,390 ± 107 cal yr BP (Zillén et al., 2002), respectively. Independent age control for the Hekla-4 cryptotephra in TSK is provided by an accelerator mass spectrometer (AMS) ^{14}C date (Poznan radiocarbon laboratory, sample POZ-55885) of a small twig located just 12 cm above the glass shard findings at 595 cm depth. The calibrated age of 4196 ± 182 cal yr BP (3800 ± 35 ^{14}C yr BP) of the macrofossil remain corresponds well with the published age estimates for the Hekla-4 eruption and thus supports the correlation to this event.

Sample TSK11_B2o_84-85_T (Glen Garry?)

Two shards cm^{-3} were found in sample TSK11_B2o_84-85_T in non-laminated sediments at 401.4 cm composite depth. The major element data of one of these colourless, highly vesicular shards indicate a high silica rhyolitic composition with relatively high silica (ca 77 wt%) and low K_2O (ca 2.0 wt%) concentrations that resembles that of the late Holocene Glen Garry Tephra (GGT) (Fig 4c). The GGT was first detected in peat deposits in central Scotland (Dugmore et al., 1995a) and radiocarbon dated at 2,088 ± 122 cal yr BP (Barber et al., 2008). The source of the GGT has not been identified yet, but geochemical similarities with the 2 ka Askja tephra point to the Dyngjufjöll volcanic system (Barber et al., 2008) (Fig. 4c). The GGT was recently also identified and OSL dated at 2.1 ± 0.1 ka in the Mirkovice 33 archaeological site in NW Poland (Housley et al., 2013b) (Fig. 5). However, the correlation of the Glen Garry tephra in TSK sediments is based only on one single analytical point and thus needs further proof. Therefore, we only tentatively attribute this glass shard to this event mainly based on its dating in TSK sediments at ca 2100 cal yr BP (Fig. 6).

Sample TSK11_B1u_137-142_T (unknown Grimsvötn?)

Two brown, low vesicular glass shards occur in sample TSK11_B1u_137-142_T between 237.7 and 243.5 cm composite depth (240.6 cm mid-point composite depth). This basaltic cryptotephra is located in the uppermost, non-laminated sediments of the TSK record and dates between ca 1060±75 and 1094±75 cal yr BP (~AD890 - AD856) according to varve supported sedimentation rate estimates. During historical times, at least three basaltic eruptions occurred from Icelandic volcanoes with widespread tephra dispersal, i.e. the AD870 Landnám eruption from the Vatnaöldur crater, the AD~934 Eldgjá fissure eruption in the Eastern Volcanic Zone and the AD1477 Veiðivötn eruption (Larsen et al., 1999; Larsen et al., 2002; Óladóttir et al., 2011). The major element chemistry of the TSK tephra, however, does not match the composition of either of those tephra, but shows a strong affinity to the Grimsvötn system due to the typical high TiO_2 concentrations of ca 2.8 wt% (Fig. 4b). Larsen (1984) noted Grimsvötn activity between the Landnám and Eldgjá eruptions; furthermore, still emerging medial-distal tephra data indicate that the Grimsvötn system produced at least six individual tephra layers with almost identical glass composition during this time interval (Óladóttir et al., 2011) (Fig. 4b). Therefore, and because of the low number of detected glass shards in TSK sediments prevents from an attribution to a specific event.

Sample TSK11_K3_33-34_T (Askja-AD1875)

The uppermost cryptotephra in the TSK sequence, TSK11_K3_33-34_T, occurs in 46.7 cm composite depth and encompasses at least 40 colourless to light brownish glass shards (Fig.

3). The cryptotephra is positioned in non-laminated sediments ca 9 cm below the topmost well-varved interval which dates between AD2010 and AD1924 (Kienel et al., 2013). The major element composition of glass shards is heterogeneous rhyolitic with two populations that mainly differ in CaO (2.3-2.8 wt% vs. 3.2-3.4 wt %) and FeO (3.1-3.9 wt% vs. 4.5-4.8 wt%) concentrations (Table 1). The glass chemistry shows some affinity to the Glen Garry Tephra with slightly higher TiO_2 (ca 0.7-1.2 wt%) and MgO (ca 0.7-1.0 wt%) contents. Several historical, silicic and widespread eruptions before AD1924 are reported from Iceland, i.e. Askja-AD1875, Hekla AD1510, Öræfajökull AD1362 and Hekla-AD1104 (e.g. Larsen et al., 1999; 2002; Óladóttir et al., 2011). The best geochemical match of tephra TSK11_K3_33-34_T is given for the Askja-AD1875 tephra (Fig. 4a). The Plinian Askja-AD1875 eruption occurred at the Dyngjufjöll volcanic centre in NE Iceland and resulted in the formation of the Öskjuvatn caldera, which is nested within the larger and older (10-ka) Askja caldera (e.g. Sigurdsson and Sparks, 1978, 1981). Askja-AD1875 was one of the largest historical eruption on Iceland with a magnitude of VEI 5 (http://www.volcano.si.edu; Carey et al., 2009). The main eruption started on March 28th 1875 and produced a series of subplinian fallout (Unit B), phreatoplinian fall (Unit C1) and flow (Unit C2) and Plinian fallout deposits (Unit D) (Carey et al., 2009; Self and Sparks, 1978). Tephra from units C and subunits D1, D3 and D5 were widely dispersed towards the East and Southeast over Scandinavia (Carey et al., 2009; Mohn, 1878) and have been found in numerous lake and peat records in Norway (e.g. Pilcher et al., 2005), Sweden (e.g. Bergman et al., 2004; Boygle, 1998; Davies et al., 2007; Oldfield et al., 1997; Wastegård, 2005; Wastegård and Davies, 2009), and possibly N central Germany (Van den Bogaard and Schmincke, 2002) (Fig. 5). The composition of the Askja-AD1875 tephra in TSK sediments is similar to that of other distal tephras and that of proximal Unit D fallout deposits (Fig. 4a). The Askja-AD1875 tephra is an excellent time marker in TSK sediments that allows the precise synchronization with palaeoenvironmental records from Scandinavia and across the western and central Baltic region.

4.2 Lake Czechowskie Holocene tephrostratigraphy

Sample JC12_D6_112-113_T (Hässeldalen)

The lowermost cryptotephra JC12_D6_112-113_T in Lake Czechowskie is embedded in laminated sediments in 1158.5 cm composite depth, 18 cm above the biostratigraphically defined Younger Dryas/Holocene transition (Ott et al., submitted). The tephra exhibited 3 colourless, high-vesicular shards cm^{-3}, which all show a rhyolitic composition. The major element glass chemistry is characterized by relatively low FeO (ca 1.2 wt%) and CaO (ca 0.5 wt%) contents, as well as high SiO_2 (77.9-78.3 wt%) and K_2O (3.9-4.5 wt%) concentrations. The glass chemical composition in combination with the stratigraphic position of tephra JC12_D6_112-113_T above the Younger Dryas/Holocene boundary suggest a correlation with the early Holocene Hässeldalen tephra (HDT; 11,380 ± 216 cal yr BP; Wohlfarth et al., 2006) (Fig. 4f) and is also comparable to tephra TSK13_F6_99-100_T from Lake Tiefer See. The HDT represents an isochron for the synchronization of JC and TSK sediment records ca. 200 years after the onset of the Holocene.

Sample JC12_D6_95-95.5_T (Askja-S)

Cryptotephra JC12_D6_95-95.5_T is positioned in laminated sediments in 1141.25 cm composite depth, ca 17 cm above the Hässeldalen Tephra. It contained 22 colourless, high vesicular to cuspate glass shards cm^{-3} (Fig. 3), of which 13 shards have been geochemically analysed. The major element chemistry revealed a homogeneous, high silica (76.2-77.1 wt%) rhyolitic composition that matches best the glass compositions of the early Holocene Askja-S tephra (Fig. 4d). Since it further resembles the Tiefer See tephra TSK13_F6_91-92_T both lake records can be unequivocally synchronized using this cryptotephra.

Samples JC09_B2_170-173_T and JC09_B2_155-158_T (unknown Icelandic?)

Two cryptotephras of identical composition have been identified in varved late Holocene JC sediments in 495.5 cm and 480.5 cm composite depth. Samples JC09_B2_170-173_T and JC09_B2_155-158_T exhibited 2 and 6 shards per 3-cm^3-sediment sample, respectively. All shards are colourless, highly vesicular and of high silica rhyolitic composition (Fig. 4c). Preliminary varve counting suggests a deposition of cryptotephras at 1960 ± 20 varve yr BP and 1890 ± 20 varve yr BP, respectively. Comparison with major element glass data of proximal and distal tephras from Iceland and Jan Mayen from this time period suggests a tentative match with the high-silica glass population of the DOM-4 tephra (ca 1550 interpolated ^{14}C yr BP) from Dosenmoor in N Germany (van den Bogaard and Schmincke, 2002) (Fig. 4c). DOM-4 has been assigned to unknown Icelandic silicic activities (van den Bogaard and Schmincke, 2002). Therewith, tephras JC09_B2_170-173_T and JC09_B2_155-158_T cannot be used as isochrones for synchronization.

Sample JC12_K2_35-36_T (Askja-AD1875)

The uppermost cryptotephra JC12_K2_35-36_T is located in varved sediments in 48.5 cm composite depth. It revealed ten colourless to light brownish, high-vesicular glass shards (Fig. 3) of homogenous rhyolitic composition. The major element glass chemistry strongly resembles that of the less evolved glass population of tephra TSK_K3_33-34_T and the proximal Askja-AD1875 tephra deposits (Fig. 4a). The Askja-AD1875 tephra in Lake Czechowskie sediments is the first finding in Polish sites (Wulf et al., 2014). It provides an excellent correlation marker for the comparison of historical palaeoenvironmental data with Lake Tiefer See as well as other records.

4.3 Tephrochronologies

4.3.1 Lake Tiefer See

One visible tephra layer and seven cryptotephras have been identified in the sediment sequence of Lake Tiefer See. Six of these tephras were correlated with dated erupted events and thus represent well-suited time markers for the construction of a detailed tephrochronology of TSK sediments (Fig. 6a). The possible Hässeldalen and Askja-S tephras likely represent anchor points for the non-laminated early Holocene interval. The Saksunarvatn Ash layer (10,210 ± 35 cal yr BP), Lairg-B (6,683 ± 45 cal yr BP) and Hekla-4 (4293 ± 43 cal yr BP) cryptotephras represent isochrones for the floating varved early to mid-Holocene intervals. The historical Askja-AD1875 tephra forms an essential time marker for the validation of sedimentation rate estimates in the partially non-laminated, late Holocene sediments. The tentatively assigned Glen Garry Tephra (2,088 ± 122 cal yr BP) is not used in the TSK age model since tephrochronological correlation still needs further proof. Based on the tephrochronological results, a preliminary chronology is constructed for the TSK sediment sequence. This chronology will be compared in detail with the on-going independent dating based on varve counting, sedimentation rate estimates and radiocarbon dating. Presently, we can roughly infer mean sedimentation rates of ~0.7 mm/yr for the mid-Holocene since the deposition of the Hekla-4 tephra and 1.0 mm/yr up to 3.5 mm/yr during the late Holocene and recent time periods, respectively.

4.3.2 Lake Czechowskie

Five cryptotephra horizons have been identified in Lake Czechowskie sediments, of which three tephras provide robust anchor points for the JC chronology (Fig. 6b). The early Holocene Askja-S and the likely Hässeldalen tephras are especially important since they represent isochrones within the floating varved section between ca 12 m and 11 m composite depth. The Askja-AD1875 tephra is a time marker for the varved sediments of historical times and is applicable to validate varve counts in sub-recent sediments. Based only on the tephra occurrences we can calculate rough and average sedimentation rates for the Holocene (ca 1 mm/yr) and historical times after the Askja-AD1875 tephra (ca 3.6 mm/yr). However, the limited number of tephra anchor points obviously does not allow more detailed measurements of the variability.

4.4 Tephra dispersal in central and northern Europe

The tephra findings in the partially varved sediment records of Lake Tiefer See and Lake Czechowskie provide the potential to directly compare palaeoclimate information of these records with other high-resolution data from continental Central and Northern Europe. First examples from comparisons of varved Lateglacial records along E-W (Lake Meerfelder Maar, Rehwiese and Trzechowskie palaeolakes; Słowiński et al., 2014; Wulf et al., 2013) and N-S transects (Lakes Meerfelder Maar and Kråkenes; Lane et al., 2013; Rach et al., 2014) have demonstrated the capability of detangling temporal and spatial offsets of palaeoenvironmental and palaeoecological responses to past abrupt climate changes by using tephra isochrones. With the new results presented here, it is possible to extend these comparisons to the Holocene and historical time periods (Fig. 7).

The Askja-S and likely the Hässeldalen tephras are unequivocal marker layers for the synchronization of early Holocene sediment records. The number of sites where they have been found, however, is restricted to a few records in northern and central Europe (Fig. 5). Therefore our new findings in the TSK and JC records are a further addition to the construction of a more detailed dispersal map (Fig. 5). Their occurrences in the Polish site even are of particular interest, since this is, on the one hand, the furthest south-easterly dispersal so far (Fig. 5). Furthermore, the Hässeldalen and Askja-S tephras in Lake Czechowskie are the first occurrences in annually laminated sediments, thus allowing to apply a differential dating for estimating the time span between these two eruptions (Ott et al., submitted).

The finding of the visible Saksunarvatn Ash in the TSK record, in turn, is in agreement with previous finds in NE Germany (Merkt et al., 1993; Bramham-Law et al., 2013) and thus confirms the proposed dispersal map by Davies et al. (2012) (Fig. 5). The Lairg-B and Hekla-4 tephra occurrences in TSK are the furthest towards the southeast and, similar to the likely Glen Garry tephra, supplements the previous findings in northern central Germany. The distribution of the historical Askja-AD1875 tephra has been eye-witnessed and described by an initial easterly dispersal axis that changed over Sweden into a southerly direction (Mohn, 1878; Carey et al., 2009). However, findings of this tephra in sedimentary repositories are mainly restricted to Norway and Sweden; a single occurrence in N Germany is still debated (van den Bogaard and Schmincke, 2002). With the unambiguous identification of the Askja-AD1875 tephra in TSK and JC sediments we confirm the southerly dispersal direction and extend the distribution limit further to the east than previously supposed (Fig. 5).

5. Conclusions

The recently developed methods for cryptotephra identification allowed detecting and geochemical fingerprinting of thirteen cryptotephras from at least ten distinct eruptions of Icelandic volcanoes in the Holocene sediments of Lake Tiefer See and Lake Czechowskie. Half of cryptotephras are characterized by very low glass shard concentrations (e.g. 1-3 shards per 1-5 cm^3 sediment samples) due to the extreme distal location of investigated sites. Those shards are interpreted as primary deposits based on (1) the lack of findings in over- and underlying samples and (2) the non-disturbed and varved character of Holocene sediments. We need to stress, however, that further shard findings and geochemical analyses are needed to enhance the reliability of some of our tephra correlations. Accordingly, we used mainly tephras with higher shard concentrations, i.e. the Askja-AD1875, Saksunarvatn and Askja-S tephras, to construct reliable tephrochronologies that will, on the one hand, validate established varve chronologies and, on the other hand, provide valuable anchor points for chronologies of intercalated varved and non-varved sections. In addition, these tephrochronologies are a prerequisite for the synchronization of proxy data from sediment records in the southern Baltic region and beyond, which was recently stresses by the INTIMATE (INTegrating Ice core, Marine and TErrestrial records) group (Feurdean et al.; 2014). The cryptotephra findings especially in Lake Czechowskie evidence a further eastward dispersal of Lateglacial and Holocene volcanic ash from Iceland than previously proposed. Moreover, our results demonstrate the great potential also for other recently reported varved lake sediment records from northern Poland (Kinder et al., 2013; Tylmann et al., 2013a; 2013b) and the key palaeoclimate records from Lake Gościąż and Perespilno (Goslar et al., 1999; Goslar et al., 1993).

Acknowledgments

We are grateful to the German-Polish team, Brian Brademann, Robert Schedel, Michael Köhler (MKfactory), Stefan Lauterbach, Robert Weißbach, Mateusz Kramkowski, Sebastian Tyszkowski, and Jarosław Kordowski, for sediment coring in lakes Tiefer See and Lake Czechowskie. Andreas Hendrich kindly helped with the improvement of the figure design. We especially thank our student helpers for tephra sample processing, namely Katharina Schorling, Alexander Adams, Nadine Schilling, Nathalie Dust, and Yevheniia Korniienko. We thank Jörg Gast and Ralf Koch from the Naturpark Nossentiner Schwinzer Heide and the mayor Reinhard Block of the village Neu Gaarz for support. We are furthermore very grateful to two anonymous journal reviewers for their constructive comments on our manuscript. This study has been financed by the Virtual Institute of Integrated Climate and Landscape Evolution Analysis –ICLEA–, grant number VH-VI-415, of the Helmholtz Association and the National Science Centre, Poland (grants no. NN306085037 and 2011/01/B/ST10/07367). It is further a contribution to the climate initiative REKLIM Topic 8 “Abrupt climate change

derived from proxy data" and has used infrastructure of the Terrestrial Environmental Observatory (TERENO), both of the Helmholtz Association.

References

Aarnes, I., Bjune, A.E., Birks, H.H., Balascio, N.L., Bakke, J., Blaauw, M., 2012. Vegetation responses to rapid climatic changes during the last deglaciation 13,500-8,000 years ago on southwest Andoya, arctic Norway. Vegetation History and Archaeobotany 21, 17-35.

Abbott, P.M., Davies, S.M., 2012. Volcanism and the Greenland ice-cores: the tephra record. Earth-Science Reviews 115, 173-191.

Andersson, S., Rosqvist, G., Leng, M.J., Wastegård, S., Blaauw, M., 2010. Late Holocene climate change in central Sweden inferred from lacustrine stable isotope data. Journal of Quaternary Science 25, 1305-1316.

Andrews, J.T., Geirsdóttir, A., Hardardóttir, J., Principato, S., Grönvold, K., Kristjansdóttir, G.B., Helgadóttir, G., Drexler, J., Sveinbjörnsdóttir, A., 2002. Distribution, sediment magnetism and geochemistry of the Saksunarvatn (10,180 +/- 60 cal.yr BP) tephra in marine, lake, and terrestrial sediments, northwest Iceland. Journal of Quaternary Science 17, 731-745.

Barber, K., Langdon, P., Blundell, A., 2008. Dating the Glen Garry tephra: a widespread late Holocene marker horizon in the peatlands of northern Britain. Holocene 18, 31-43.

Bergman, J., Wastegård, S., Hammarlund, D., Wohlfarth, B., Roberts, S.J., 2004. Holocene tephra horizons at Klocka Bog, west-central Sweden: aspects of reproducibility in subarctic peat deposits. Journal of Quaternary Science 19, 241-249.

Birks, H.H., Gulliksen, S., Haflidason, H., Mangerud, J., 1996. New radiocarbon dates for the Vedde Ash and the Saksunarvatn Ash from Western Norway. Quaternary Research 45, 119-127.

Błaszkiewicz, M., 2005. Późnoglacjalna i wczesnoholoceńska ewolucja obniżeń jeziornych na Pojezierzu Kociewskim (wschodnia część Pomorza). Warszawa IGiPZ PAN.

Błaszkiewicz, M., 2011. Timing of the final disappearance of permafrost in the central European Lowland, as reconstructed from the evolution of lakes in N Poland. Geological Quarterly 55, 361-374.

Błaszkiewicz, M., Piotrowski, J.A., Brauer, A., Gierszewski, P., Kordowski, J., Kramkowski, M., Lamparski, P., Lorenz, S., Noryskiewicz, A.M., Ott, F., Słowinski, M., Tyszkowski, S., 2015. Climatic and morphological controls on diachronous postglacial lake and river valley evolution in the area of the Last Glaciation, northern Poland. Quaternary Science Reviews 109, 13-27.

Boygle, J., 1998. A little goes a long way: discovery of a new mid-Holocene tephra in Sweden. Boreas 27, 195-199.

Bramham-Law, C.W.F., Theuerkauf, M., Lane, C.S., Mangerud, J., 2013. New findings regarding the Saksunarvatn Ash in Germany. Journal of Quaternary Science 28, 248-257.

Brauer, A., Endres, C., Negendank, J.F.W., 1999. Lateglacial calendar year chronology based on annually laminated sediments from Lake Meefelder Maar, Germany. Quaternary International 61, 17-25.

Bronk Ramsey, C., Albert, P.G., Blockley, S.P.E., Hardiman, M., Housley, R.A., Lane, C.S., Lee, S., Matthews, I.P., Smith, V.C., Lowe, J.J., 2015. Improved age estimates for key Late Quaternary European tephra horizons in the RESET lattice. Quaternary Science Reviews. doi:10.1016/j.quascirev.2014.11.007

Carey, R.J., Houghton, B.F., Thordarson, T., 2009. Tephra dispersal and eruption dynamics of wet and dry phases of the 1875 eruption of Askja Volcano, Iceland. Bulletin of Volcanology 48, 109-125.

Chambers, F.M., Daniell, J.R.G., Hunt, J.B., Molloy, K., O'Connell, M., 2004. Tephrostratigraphy of An Loch Mór, Inis Oirr, western Ireland: implications for Holocene tephrochronology in the northeastern Atlantic region. The Holocene 14, 703-720.

Davies, S.M., Abbott, P.M., Pearce, N.J.G., Wastegård, S., Blockley, S.P.E., 2012. Integrating the INTIMATE records using tephrochronology: rising to the challenge. Quaternary Science Reviews 36, 11-27.

Davies, S.M., Elmquist, M., Bergman, J., Wohlfarth, B., Hammarlund, D., 2007. Cryptotephra sedimentation processes within two lacustrine sequences from west central Sweden. The Holocene 17, 1-13.

Davies, S.M., Wastegård, S., Wohlfarth, B., 2003. Extending the limits of the Borrobol Tephra to Skandinavia and detection of new early Holocene tephras. Quaternary Research 59, 345-352.

Dörfler, W., Feeser, I., van den Bogaard, C., Dreibrodt, S., Erlenkeuser, H., Kleinmann, A., Merkt, J., Wiethold, J., 2012. A high-quality annually laminated sequence from Lake Belau, Northern Germany: Revised chronology and its implications for palynological and tephrochronological studies. The Holocene 22, 1413-1426.

Dräger, N., Wulf, S., Kienel, U., Dulski, P., Ott, F., Slowinski, M., Theuerkauf, M., Brauer, A., 2014. High-resolution microfacies analysis and tephrochronology of varved sediments from Lake Tiefer See (NE Germany), Geophysical Research Abstracts, pp. EGU2014-2411.

Dugmore, A.J., Shore, J.S., Cook, G.T., Newton, A.J., Edwards, K.J., Larsen, G., 1995a. The radiocarbon dating of Icelandic tephra layers in Britain and Iceland. Radiocarbon 37, 379-388.

Dugmore, A.J., Larsen, G., Newton, A.J., 1995b. Seven tephra isochrones in Scotland. The Holocene 5 (3), 257-266.

Eiríksson, J., Knudsen, K.L., Haflidason, H., Heinemeier, J., 2000. Chronology of late Holocene climatic events in the northern North Atlantic based on AMS 14C dates and tephra markers from the volcano Hekla, Iceland. Journal of Quaternary Science 15 (6), 573-580.

Enters, D., Kirilova, E., Lotter, A.F., Lücke, A., Parplies, J., Jahns, S., Kuhn, G., Zolitschka, B., 2010. Climate change and human impact at Sacrower See (NE Germany) during the past 13,000 years: a geochemical record. Journal of Paleolimnology 43, 719-737.

Feurdean, A., Perşoiu, A., Tanţău, I., Stevens, T., Magyari, E.K., Onac, B.P., Marković, S., Andrič, M., Connor, S., Fărcaş, S., Gałka, M., Gaudeny, T., Hoek, W., Kolaczek, P., Kuneš, P., Lamentowicz, M., Marinova, E., Michczyńska, D.J., Perşoiu, I., Płóciennik, M., Słowiński, M., Stancikaite, M., Sumegi, P., Svensson, A., Tămaş, T., Timar, A., Tonkov, S., Toth, M., Veski, S., Willis, K.J., Zernitskaya, V., 2014. Climate variability and associated vegetation response throughout Central and Eastern Europe (CEE) between 60 and 8 ka. Quaternary Science Reviews 106, 206-224.

Froggatt, P.C., Lowe, D.J., 1990. A review of late Quaternary silicic and some other tephra formations from New Zealand: Their stratigraphy, nomenclature, distribution, volume, and age. New Zealand Journal of Geology and Geophysics 33 (1), 89-109.

Goslar, T., Balaga, K., Arnold, M., Tisnerat, N., Starnawska, E., Kuzniarski, M., Chrost, L., Walanus, A., Wieckowski, K., 1999. Climate-related variations in the composition of the lateglacial and early Holocene sediments of Lake Perespilno (eastern Poland). Quaternary Science Reviews 18, 899-911.

Goslar, T., Kuc, T., Ralska-Jasiewiczowa, M., Rozanski, K., Arnold, M., Bard, E., van Geel, B., Pazdur, M.F., Szeroczynska, K., Wicik, B., Wieckowski, K., Walanus, A., 1993. High-resolution lacustrine record of the Late Glacial/Holocene transition in central Europe. Quaternary Science Reviews 12, 287-294.

Grönvold, K., Jóhannesson, H., 1984. Eruption in Grimsvötn 1983. Course of events and chemical studies of the tephra. Jökull 34, 1-11.

Grönvold, K., Óskarsson, N., Johnsen, S.J., Clausen, H.B., Hammer, C.U., Bond, G., Bard, E., 1995. Ash layers from Iceland in the Greenland GRIP ice core correlated with oceanic and land sediments. Earth and Planetary Science Letters 135, 149-155.

Guðmundsdóttir, E.R., Eiríksson, J., Larsen, G., 2011. Identification and definition ofprimary and reworked tephra in late Glacial and Holocene marine shelf sediments off North Iceland. Journal of Quaternary Science 26, 589-602.

Haflidason, H., Sejrup, H.P., Jones, G.A., 1990. Tephra-, bio- and lithostratigraphy of an AMS dated core from the Norway basin, southern Norwegian Sea. Geonytt 17, 52.

Housley, R.A., MacLeod, A., Nalepka, D., Jurochnik, A., Masojc, M., Davies, L., Lincoln, P.C., Bronk Ramsey, C., Gamble, C.S., Lowe, J.J., 2013a. Tephrostratigraphy of a Lateglacial lake sediment sequence at Węgliny, southwest Poland. Quaternary Science Reviews 77, 4-18.

Housley, R.A., MacLeod, A., Armitage, S.J., Kabacinski, J., Gamble, C.S., 2013b. The potential of cryptotephra and OSL dating for refining the chronology of open-air archaeological windblown sand sites: a case study from Mirkowice 33, northwest Poland. Quaternary Geochronology 20, 99-108.

Hunt, J.B., Hill, P.G., 1996. An inter-laboratory comparison of the electron probe microanalysis of glass geochemistry. Quaternary International 34-36, 229-241.

Jennings, A., Thordarson, T., Zalzal, K., Stoner, J., Hayward, C., Geirsdóttir, Á., Miller, G., 2014. Holocene tephra from Iceland and Alaska in SE Greenland Shelf sediments. Geological Society, London, Special Publications 398, 157-193.

Jóhannesdóttir, G.E., Thordarson, T., Geirsdóttir, A., Larsen, G., 2005. The widespread ~10 ka Saksunarvatn tephra: a product of three large basaltic phreatoplinian eruptions?. Geophysical Research Abstracts 7. 05991 (SRef-ID:1607-7962/gra/EGU05-A.-05991).

Jóhansen, J., 1985. Studies in the Vegetation History of the Faroe and Shetland Islands. Føroya Fróðskaparfelag: Tórshavn, Faroe Islands.

Juvigné, E.H., Kozarski, S., Nowaczyk, B., 1995. The occurrence of Laacher See Tephra in Pomerania, NW Poland. Boreas 24, 225-231.

Kaiser, K., Lorenz, S., Germer, S., Juschus, O., Küster, M., Libra, J., Bens, O., Hüttl, R. F., 2012. Late Quaternary evolution of rivers, lakes and peatlands in northeast Germany reflecting past climatic and human impact – an overview. E&G Quaternary Science Journal 61, 103-132.

Kienel, U., Dulski, P., Ott, F., Lorenz, S., Brauer, A., 2013. Recently induced anoxia leading to the preservation of seasonal laminae in two NE-German lakes. Journal of Paleolimnology 50, 535-544.

Kinder, M., Tylmann, W., Enters, D., Piotrowska, N., Poręba, G., Zolitschka, B., 2013. Construction and validation of calendar-year time scale for annually laminated sediments – an example from Lake Szurpiły (NE Poland). GFF, 135: 248-257.

Kuehn, S.C., Froese, D.G., Shane, P.A.R., Participants, I.I., 2011. The INTAV intercomparison of electron-beam microanalysis of glass by tephrochronology laboratories: Results and recommendations. Quaternary International 246, 19-47.

Kylander, M.E., Lind, E.M., Wastegård, S., Löwemark, L., 2012. Recommendations for using XRF core scanning as a tool in tephrochronology. The Holocene 22(3), 371-375.

Lane, C.S., Blockley, S.P.E., Bronk Ramsey, C., Lotter, A.F., 2011a. Tephrochronology and absolute centennial scale synchronisation of European and Greenland records for the last glacial to interglacial transition: a case study of Soppensee and NGRIP. Quaternary International 246, 145-156.

Lane, C.S., De Klerk, P., Cullen, V.L., 2011b. A tephrochronology for the last lateglacial palynological record of the Endinger Bruch (Vorpommern, north-east Germany). Journal of Quaternary Science 27, 141-149.

Lane, C.S., Blockley, S.P.E., Mangerud, J., Smith, V.C., Lohne, O.S., Tomlinson, E.L., Matthews, I.P., Lotter, A.F., 2012. Was the 12.1 ka Icelandic Vedde Ash one of a kind? Quaternary Science Reviews 33, 87-99.

Lane, C.S., Brauer, A., Blockley, S.P.E., Dulski, P., 2013. Volcanic ash reveals time-transgressive abrupt climate change during the Younger Dryas. Geology 41, 1251-1254.

Larsen, G., 1982. Gjóskutímatal Jökuldals og nágrennis, In: Thórarinsdóttir, H., Óskarsson, Ó.H., Steinthórsson, S., Einarsson, T. (Eds.), Eldur er í Norðri. Sögufélag, Reykjavík, Sögufélag, Reykjavík, pp. 51-65.

Larsen, G., 1984. Recent volcanic history of the Veidivötn fissure swarm, southern Iceland - an approach to volcanic risk assessment. Journal of Volcanology and Geothermal Research 22, 33-58.

Larsen, G., Dugmore, A., Newton, A.J., 1999. Geochemistry of historical-age silicic tephras in Iceland. The Holocene 9, 463-471.

Larsen, G., Eiríksson. J., Knudsen, K.L., Heinemeier, J., 2002. Correlation of late Holocene terrestrial and marine tephra markers, north Iceland: implications for reservoir age changes. Polar Research 21 (2), 283-290.

Larsen, G., Thorarinsson, S., 1977. H4 and other acid Hekla tephra layers. Jökull 27, 28-46.

Larsen, J.J., Noe-Nygaard, N., 2014. Lateglacial and early Holocene tephrostratigraphy and sedimentology of the Store Slotseng basin, SW Denmark: a multi-proxy study. Boreas 43, 349-361.

Lawson, I.T., Swindles, G.T., Plunkett, G., Greenberg, D., 2012. The spatial distribution of Holocene cryptotephras in north-west Europe since 7 ka: implications for understanding ash fall events from Icelandic eruptions. Quaternary Science Reviews 41, 57-66.

Lilja, C., Lind, E.M., Morén, B., Wastegård, S., 2013. A Lateglacial-early Holocene tephrochronology for SW Sweden. Boreas 42, 544-554.

Lind, E.M., Wastegård, S., 2011. Tephra horizons contemporary with short early Holocene climate fluctuations: New result from the Faroe Islands. Quaternary International 246.

Lind, E.M., Wastegård, S., Larsen, J.J., 2013. A Late Younger Dryas-Early Holocene tephrostratigraphy for Fosen, Central Norway. Journal of Quaternary Science 28, 803-811.

Lohne, O.S., Mangerud, J., Birks, H.H., 2013. Precise ^{14}C ages of the Vedde and Saksunarvatn ashes and the younger Dryas boundaries from western Norway and their comparison with the Greenland Ice Core (GICC05) chronology. Journal of Quaternary Science 28, 490-500.

Loon, A.J.v., Błaszkiewicz, M., Degórski, M., 2012. The role of permafrost in shaping the Late Glacial relief of northern Poland. Netherlands Journal of Geosciences 91, 223-231.

Lowe, D.J., 2011. Tephrochronology and its application: A review. Quaternary Geochronology 6, 107-153.

Mangerud, J., Furnes, H., Jóhansen, J., 1986. A 9000-year-old ash bed on the faroe islands. Quaternary Research 26, 262-265.

Marks, L., 2012. Timing of the Late Vistulian (Weichselian) glacial phases in Poland. Quaternary Science Reviews 44, 81-88.

Meara, R.H., 2012. Geochemical fingerprinting of Icelandic silicic Holocene tephra layers, College of Science and Engineering. University of Edinburgh, p. 338 pp.

Merkt, J., Müller, H., 1999. Varve chronology of Lateglacial in Northwest Germany from lacustrine sediments of the Hämelsee/Lower Saxony. Quaternary International 61, 41-59.

Merkt, J., Müller, H., Knabe, W., Müller, P., Weiser, T., 1993. The early Holocene Saksunarvatn Tephra found in lake sediments in N.W. Germany. Boreas 22, 93-100.

Mohn, H., 1878. Askeregnen den 29de-30-te Marts 1875. Forhandlinger I Videnskapsselskabet I Christiania aar 1877 10, 89-92.

Mortensen, A.K., Bigler, M., Grönvold, K., Steffensen, J.P., Johnsen, S.J., 2005. Volcanic ash layers from the Last Glacial Termination in the NGRIP ice core. Journal of Quaternary Science 20, 209-219.

Neugebauer, I., Brauer, A., Dräger, N., Dulski, P., Wulf, S., Plessen, B., Mingram, J., Herzschuh, U., Brande, A., 2012. A Younger Dryas varve chronology from the Rehwiese palaeolake record in NE-Germany. Quaternary Science Reviews 36, 91-102.

Óladóttir, B.A., Sigmarsson, O., Larsen, G., Thordarson, T., 2008. Katla volcano, Iceland: magma composition, dynamics and eruption frequency as recorded by Holocene tephra layers. Bulletin of Volcanology 70, 475-493.

Óladóttir, B.A., Larsen, G., Sigmarsson, O., 2011. Holocene volcanic activity at Grímsvötn, Bádarbunga and Kverkfjöll subglacial centres beneath Vatnajökull, Iceland. Bulletin of Volcanology. DOI 10.1007/s00445-011-0461-4.

Oldfield, F., Thompson, R., Crooks, P.R.J., Gedye, S.J., Hall, V.A., Harkness, D.D., Housley, R.A., McCormac, F.G., Newton, A.J., Pilcher, J.R., Renberg, I., Richardson, N., 1997. Radiocarbon dating of a recent high latitude peat profile: Stor Amyran, northern Sweden. The Holocene 7, 283-290.

Ott, F., Brauer, A., Slowinski, M., Wulf, S., Putyrskaya, V., Blaszkiewicz, M., 2014. Constructing a precise and robust chronology for the varved sediment record of Lake Czechowskie (Poland), Geophysical Research Abstracts, pp. EGU2014-10328.

Ott, F., Wulf, S., Serb, J., Słowiński, M., Obremska, M., Błaszkiewicz, M., Brauer, A., submitted. Constraining the time span between the early Holocene Hässeldalen and Askja-S Tephras through varve counting in the Lake Czechowskie sediment record, Poland. Journal of Quaternary Science.

Pilcher, J.R., Hall, V.A., McCormac, F.G., 1996. An outline tephrochronology for the Holocene of the north of Ireland. Journal of Quaternary Science 11 (6), 485-494.

Pilcher, J.R., Bradley, R.S., Francus, P., Anderson, L., 2005. A Holocene tephra record from the Lofoten Islands, Arctic Norway. Boreas 34, 136-156.

Pyne-O'Donnell, S.D.F., Blockley, S.P.E., Turney, C.S.M., Lowe, J.J., 2008. Distal volcanic ash layers in the Lateglacial Interstadial (GI-1): problems of stratigraphic discrimination. Quaternary Science Reviews 27, 72-84.

Rach, O., Brauer, A., Wilkes, H., Sachse, D., 2014. Delayed hydrological response to Greenland cooling at the onset of the Younger Dryas in western Europe. Nature Geoscience 7, 109-112.

Ranner, P.H., Allen, J.R.M., Huntley, B., 2005. A new early Holocene cryptotephra from northwest Scotland. Journal of Quaternary Science 20, 201-208.

Rasmussen, S.O., Andersen, K.K., Svensson, A.M., Steffensen, J.P., Vinther, B.M., Clausen, H.B., Siggaard-Andersen, M.L., Johnsen, S.J., Larsen, L.B., Dahl-Jensen., D., Bigler, M., Röthlisberger, R., Fischer, H., Goto-Azuma, K., Hanssom, M.E., Ruth, U., 2006. A new Greenland ice core chronology for the last glacial termination. Journal of Geophysical Research D: Atmospheres, 111.

Rasmussen, S.O., Bigler, M., Blockley, S.P., Blunier, T., Buchardt, S.L., Clausen, H.B., Cvijanovic, I., Dahl-Jensen, D., Johnsen, S.J., Fischer, H., Gkinis, V., Guillevic, M., Hoek, W.Z., Lowe, J.J., Pedro, J.B., Popp, T., Seierstad, I.K., Steffensen, J.P., Svensson, A.M., Vallelonga, P., Vinther, B.M., Walker, M.J.C., Wheatley, J.J., Winstrup, M., 2014. A stratigraphic framework for abrupt climatic changes during the Last Glacial period based on three synchronized Greenland ice-core records: refining and extending the INTIMATE event stratigraphy. Quaternary Science Reviews 106, 14-28.

Riede, F., Bazely, O., Newton, A.J., Lane, C.S., 2011. A Laacher See-eruption supplement to Tephrabase: Investigating distal tephra fallout dynamics. Quaternary International 246, 134-144.

Rinterknecht, V., Börner, A., Bourlès, D., Braucher, R., 2014. Cosmogenic 10Be dating of ice sheet marginal belts in Mecklenburg-Vorpommern, Western Pomerania (northeast Germany). Quaternary Geochronology 19, 42-51.

Sigurdsson, H., Sparks, R.S.J., 1978. Rifting episode in North Iceland in 1874-1875 and the eruptions of Askja and Sveinagja. Bulletin of Volcanology 41, 149-167.

Sigurdsson, H., Sparks, R.S.J., 1981. Petrology of rhyolitic and mixed magma ejecta from the 1875 eruption of Askja, Iceland. Journal of Petrology 22, 41-84.

Sigvaldason, G.E., 2002. Volcanic and tectonic processes coinciding with glaciation and crustal rebound: an early Holocene rhyolitic eruption in the Dyngjufjöll volcanic centre and the formation of the Askja caldera, north Iceland. Bulletin of Volcanology 64, 192-205.

Słowiński, M., 2010. Macrofossil reconstruction of preboreal wetland formed on dead ice block - a case study of the Borzechowo mire in East Pomerania, Poland. Studia Quaternaria 27, 3-10.

Słowiński, M., Błaszkiewicz, M., Brauer, A., Noryśkiewicz, B., Ott, F., Tyszkowski, S., in press. The role of melting dead ice on landscape transformation in the early Holocene in Tuchola Pinewoods, North Poland. Quaternary International. doi:10.1016/j.quaint.2014.06.018

Steinthórsson, S., 1977. Tephra layers in a Drill Corer from the Vatnajökull Ice cap. Jökull 27, 2-27.

Sverrisdottir, G., 2007. Hybrid magma generation preceding Plinian silicic eruptions at Hekla, Iceland: evidence from mineralogy and chemistry of two zoned deposits. Geological Magazine 144, 643-659.

Thordarson, T., Miller, D.J., Larsen, G., Self, S., Sigurdsson, H., 2001. New estimates of sulfur degassing and atmospheric mass-loading by the 934 AD Eldgjá eruption, Iceland. Journal of Volcanology and Geothermal Research 108, 33-34.

Turney, C.S.M., Harkness, D.D., Lowe, J.J., 1997. The use of microtephra horizons to correlate Late-glacial lake sediment successions in Scotland. Journal of Quaternary Science 12, 525-531.

Turney, C.S.M., van den Burg, K., Wastegård, S., Davies, S.M., Whitehouse, N.J., Pilcher, J.R., Callaghan, C., 2006. North European last glacial-interglacial transition (LGIT; 15-9 ka) tephrochronology: extended limits and new events. Journal of Quaternary Science 21, 335-345.

Tylmann, W., Enters, D., Kinder, M., Moska, P., Ohlendorf, C., Poręba, G., Zolitschka, B., 2013a. Multiple dating of varved sediments from Lake Łazduny, northern Poland: Toward an improved chronology for the last 150 years. Quaternary Geochronology 15, 98-107.

Tylmann, W., Zolitschka, B., Enters, D., Ohlendorf, C., 2013b. Laminated lake sediments in northeast Poland: distribution, preconditions for formation and potential for Paleoenvironmental investigation: Journal of Paleolimnology 50, 487–503.

Van den Bogaard, C., Dörfler, W., Glos, R., Nadeau, M.-J., Grootes, P.M., Erlenkeuser, H., 2002. Two tephra layers bracketing Late Holocene paleoecological changes in Northern Germany. Quaternary Research 57, 314-324.

Van den Bogaard, C., Schmincke, H.-U., 2002. Linking the North Atlantic to central Europe: a high-resolution Holocene tephrochronological record from northern Germany. Journal of Quaternary Science 17, 3-20.

Vinther, B.M., Clausen, H.B., Johnsen, S.J., Rasmussen, S.O., Andersen, K.K., Buchardt, S.L., Dahl-Jensen, D., Seierstad, I.K., Siggaard-Andersen, M.L., Steffensen, J.P., Svensson, A., Olsen, J., Heinemeier, J., 2006. A synchronized dating of three Greenland ice cores throughout the Holocene. Journal of Geophysical Research 111, D13102.

Wastegård, S., 2005. Late Quaternary tephrochronology of Sweden: a review. Quaternary International 130, 49-62.

Wastegård, S., Davies, S.M., 2009. An overview of distal tephrochronology in northern Europe during the last 1000 years. Journal of Quaternary Science 24, 500-512.

Wohlfarth, B., Blaauw, M., Davies, S.M., Andersson, M., Wastegård, S., Hormes, A., Possnert, G., 2006. Constraining the age of Lateglacial and early Holocene pollen zones and tephra horizons in southern Sweden with Bayesian probability methods. Journal of Quaternary Science 21, 321-334.

Wulf, S., Dräger, N., Ott, F., Serb, J., Brauer, A., 2014. Findings of historical Icelandic (Askja AD 1875) tephras in varved lake records from Lake Tiefer See and Lake Czechowskie: a new potential for synchronizing the recent environmental history in NE Germany and N central Poland. Geophysical Research Abstracts 16, EGU2014-9947.

Wulf, S., Ott, F., Slowinski, M., Noryskiewicz, A.M., Dräger, N., Martin-Puertas, C., Czymzik, M., Neugebauer, I., Dulski, P., Bourne, A.J., Blaszkiewicz, M., Brauer, A., 2013. Tracing the Laacher See Tephra in the varved sediment record of the Trzechowskie palaeolake in central Northern Poland. Quaternary Science Reviews 76, 129-139.

Zielinski, G.A., Germani, M.S., Larsen, G., Baillie, M.G.L., Whitlow, S., Twicker, M.S., Taylor, K., 1995. Evidence or the Eldgjá (Iceland) eruption in the GISP2 Greenland ice core: relationship to eruption processes and climatic conditions in the tenth century. The Holocene 5, 129-140.

Zielinski, G.A., Mayewski, P.A., Meeker, L.D., Grönvold, K., Germani, M.S., Whitlow, S., Twickler, M.S., Taylor, K., 1997. Volcanic aerosol records and tephrochronology of the Summit, Greenland, ice cores. Journal of Geophysical Research 102, 26625 - 26640.

Zillén, L.M., Wastegård, S., Snowball, I.F., 2002. Calendar year ages of three mid-Holocene tephra layers identified in varved lake sediments in west central Sweden. Quaternary Science Reviews 21, 1583-1591.

Zolitschka, B., 1990. Jahreszeitlich geschichtete Seesedimente ausgewählter Eifelmaare. Documenta naturae 60, 1-226.

Table 1: Individual, non-normalized major element glass data of cryptotephras found in Lake Tiefer See.

Sample	SiO_2	TiO_2	Al_2O_3	FeO_{tot}	MnO	MgO	CaO	Na_2O	K_2O	P_2O_5	Total	Cl	F
TSK11_K3_33-34_T	74.14	0.77	12.19	3.23	0.11	0.69	2.26	3.38	2.48	0.12	99.37	0.05	0.00
46.7 cm	74.45	0.78	12.09	3.15	0.12	0.71	2.22	3.49	2.42	0.13	99.57	0.04	0.00
Askja-AD1875	74.83	0.83	12.29	3.36	0.10	0.70	2.54	3.52	2.31	0.15	100.6	0.03	0.00
	75.72	0.91	12.36	3.11	0.08	0.66	2.31	3.12	2.44	0.12	100.8	0.03	0.00
	75.41	0.74	12.23	3.19	0.08	0.65	2.33	3.18	2.46	0.13	100.4	0.04	0.00
	75.38	0.78	12.31	3.16	0.07	0.65	2.41	3.36	2.39	0.12	100.6	0.03	0.00
	75.17	0.82	12.21	3.35	0.11	0.74	2.48	3.63	2.31	0.12	100.9	0.03	0.00
	75.19	0.78	12.54	3.42	0.12	0.71	2.55	3.60	2.30	0.14	101.3	0.04	0.00
	73.39	0.91	12.59	3.73	0.13	0.86	2.72	3.21	2.26	0.17	99.96	0.04	0.00
	73.73	0.86	12.79	3.90	0.11	0.83	2.75	3.28	2.24	0.18	100.6	0.04	0.00
	71.81	1.08	13.01	4.57	0.12	1.06	3.28	3.72	2.13	0.24	101.0	0.03	0.00
	72.45	0.99	12.45	4.77	0.12	1.02	3.36	3.43	2.07	0.25	100.9	0.03	0.00
	71.67	1.17	12.54	4.78	0.13	0.96	3.33	3.55	2.25	0.24	100.6	0.03	0.00
TSK11_B1u_137-142_T	50.55	2.73	12.87	13.10	0.24	5.79	9.44	2.89	0.51	0.33	98.46	0.01	0.00
240.6 cm	50.54	2.77	12.89	12.65	0.21	5.66	9.53	2.81	0.51	0.32	97.89	0.02	0.00
unknown Grimsvötn													
TSK11_B2o_84-85_T	72.73	0.53	12.69	3.72	0.08	0.40	2.35	3.77	1.97	0.07	98.32	0.02	0.00
401.4 cm													
Glen Garry?													
TSK11_A3_120-125_T	73.68	0.10	13.03	1.93	0.07	0.01	1.31	3.97	2.74	0.01	96.85	0.08	0.03
607.9 cm	72.56	0.12	12.80	1.94	0.12	0.04	1.32	3.71	2.70	0.01	95.32	0.07	0.00
Hekla-4													
TSK13_F5_37-43_T	69.18	0.17	13.78	2.05	0.09	0.12	0.57	5.10	4.37	0.00	95.43	0.20	0.00
791.5 cm	69.44	0.20	13.94	2.28	0.10	0.15	0.63	5.31	4.22	0.00	96.27	0.21	0.00
Lairg-B													
TSK13_F6_55_T	50.42	3.05	12.73	13.90	0.24	5.56	9.46	2.83	0.43	0.33	98.95	0.01	0.00
989.2 cm	50.14	2.99	12.71	14.19	0.21	5.63	9.69	2.65	0.40	0.32	98.94	0.02	0.00
Saksunarvatn	50.85	3.14	12.86	14.08	0.20	5.26	9.40	2.66	0.48	0.33	99.25	0.00	0.00
	51.03	3.10	12.65	14.15	0.22	5.21	9.52	2.45	0.49	0.28	99.09	0.02	0.00

	51.80	2.92	13.24	14.26	0.23	5.02	9.66	2.49	0.47	0.31	100.4	0.02	0.00
	50.58	2.83	12.97	13.35	0.27	5.71	9.90	2.64	0.42	0.37	99.03	0.02	0.00
	50.90	3.13	12.83	14.53	0.23	5.88	9.88	2.16	0.55	0.30	100.3	0.01	0.00
	50.61	2.81	12.88	13.73	0.25	5.78	9.72	2.51	0.43	0.33	99.04	0.02	0.00
	50.71	2.90	12.68	13.88	0.21	5.73	9.69	2.79	0.41	0.34	99.35	0.03	0.00
	50.77	2.89	12.97	13.73	0.22	5.62	9.87	2.51	0.40	0.32	99.30	0.00	0.00
	50.40	1.37	13.58	11.06	0.21	7.95	12.36	2.15	0.13	0.06	99.27	0.02	0.00
	50.80	2.75	12.98	13.61	0.23	5.61	9.68	2.53	0.46	0.31	98.97	0.02	0.00
	50.04	1.43	13.44	11.21	0.19	8.17	12.32	2.12	0.16	0.12	99.20	0.00	0.00
	50.15	3.08	12.42	14.01	0.21	5.69	9.56	2.77	0.49	0.31	98.69	0.02	0.00
	50.48	3.10	12.56	13.73	0.22	5.31	9.48	2.80	0.44	0.34	98.46	0.02	0.00
	50.90	3.15	12.88	14.04	0.25	5.24	9.41	2.60	0.49	0.32	99.28	0.01	0.00
	49.92	2.96	12.72	13.70	0.26	5.58	9.56	2.71	0.45	0.37	98.24	0.01	0.00
	50.10	1.55	13.69	10.90	0.18	7.82	12.56	2.08	0.13	0.13	99.14	0.01	0.00
	51.01	3.16	12.97	13.85	0.29	5.29	9.51	2.60	0.52	0.37	99.56	0.02	0.00
	50.77	3.07	12.88	13.84	0.24	5.48	9.47	2.67	0.48	0.37	99.26	0.02	0.00
	50.52	3.02	12.79	13.98	0.23	5.31	9.40	2.66	0.42	0.33	98.66	0.01	0.00
	49.92	2.89	12.79	13.82	0.24	5.87	9.74	2.76	0.45	0.29	98.77	0.02	0.00
	50.22	1.63	13.86	11.32	0.24	7.60	12.01	1.96	0.17	0.14	99.14	0.00	0.00
	50.07	2.97	13.08	14.46	0.25	5.56	9.39	2.74	0.47	0.37	99.36	0.02	0.00
	50.49	2.85	12.96	13.75	0.21	5.60	9.77	2.71	0.45	0.33	99.12	0.01	0.00
	49.89	2.83	13.01	13.84	0.19	5.92	9.89	2.73	0.43	0.30	99.03	0.01	0.00
	50.38	3.01	12.49	14.04	0.23	5.55	9.60	2.70	0.49	0.35	98.84	0.01	0.00
	49.85	3.13	12.85	13.84	0.23	5.46	9.38	2.81	0.46	0.34	98.35	0.02	0.00
	49.62	2.91	12.89	13.76	0.24	5.48	9.57	2.73	0.41	0.34	97.95	0.02	0.00
	50.07	2.81	12.96	13.43	0.27	5.97	9.82	2.57	0.42	0.34	98.66	0.01	0.00
TSK13_F6_91-92_T	74.50	0.29	11.83	2.51	0.11	0.22	1.60	3.16	2.31	0.02	96.55	0.06	0.00
1023.2 cm	75.80	0.32	12.12	2.48	0.10	0.25	1.62	3.40	2.44	0.00	98.53	0.05	0.00
Askja-S	73.37	0.28	11.80	2.41	0.09	0.25	1.53	3.21	2.44	0.00	95.38	0.05	0.00
TSK13_F6_99-100_T	76.87	0.07	11.60	1.08	0.05	0.04	0.44	3.19	4.04	0.01	97.40	0.13	0.00
1031.7 cm	76.46	0.08	11.52	1.11	0.07	0.02	0.46	3.15	3.82	0.01	96.71	0.14	0.00
Hässeldalen?													

Table 2: Individual, non-normalized major element glass data of cryptotephras found in Lake Czechowskie.

Sample	SiO_2	TiO_2	Al_2O_3	FeO_{tot}	MnO	MgO	CaO	Na_2O	K_2O	P_2O_5	Total	Cl	F
JC12_K2_35-36_T	74.44	0.78	12.43	3.39	0.10	0.74	2.38	3.87	2.22	0.12	100.47	0.04	0.00
48.5 cm	75.08	0.77	12.27	3.33	0.10	0.71	2.36	3.67	2.34	0.14	100.77	0.05	0.00
Askja-AD1875													
JC09_B2_155-158_T	74.63	0.06	12.11	0.49	0.00	0.06	0.49	3.79	4.32	0.00	95.96	0.11	0.00
480.5 cm	73.99	0.06	12.38	0.58	0.05	0.06	0.44	3.38	4.52	0.01	95.46	0.09	0.00
unknown Icelandic?	73.89	0.07	12.02	0.53	0.04	0.03	0.55	3.35	4.28	0.00	94.77	0.11	0.00
	74.22	0.09	12.18	0.49	0.09	0.06	0.51	3.81	4.20	0.00	95.64	0.11	0.00
JC09_B2_170-173_T	74.04	0.04	11.88	0.54	0.08	0.05	0.53	3.44	4.09	0.00	94.70	0.11	0.00
495.5 cm	73.71	0.08	11.96	0.52	0.06	0.06	0.51	3.48	4.18	0.01	94.58	0.10	0.00
unknown Icelandic?													
JC12_D6_95-95.5_T	74.24	0.34	12.10	2.48	0.07	0.22	1.52	4.00	2.40	0.06	97.42	0.05	0.00
1141.25 cm	73.20	0.27	11.72	2.38	0.06	0.24	1.52	3.75	2.52	0.06	95.71	0.04	0.00
Askja-S	74.04	0.31	12.43	2.60	0.10	0.23	1.58	3.49	2.40	0.02	97.21	0.03	0.00
	73.25	0.33	11.76	2.43	0.07	0.23	1.52	3.87	2.45	0.05	95.96	0.03	0.00
	75.52	0.32	12.01	2.45	0.06	0.23	1.53	3.83	2.55	0.04	98.54	0.04	0.00
	74.40	0.31	11.92	2.51	0.08	0.26	1.54	3.81	2.51	0.01	97.35	0.05	0.00
	75.75	0.31	12.24	2.53	0.09	0.23	1.58	3.79	2.39	0.01	98.91	0.05	0.00
	74.21	0.28	11.86	2.48	0.06	0.21	1.56	3.80	2.47	0.10	97.03	0.04	0.00
	74.02	0.29	11.90	2.57	0.09	0.25	1.57	3.77	2.49	0.05	97.01	0.06	0.00
	75.70	0.26	12.25	2.59	0.13	0.28	1.60	3.85	2.48	0.04	99.19	0.06	0.00
	76.11	0.28	12.13	2.49	0.10	0.26	1.54	3.53	2.49	0.00	98.93	0.06	0.00
	75.75	0.32	12.17	2.38	0.08	0.22	1.49	3.44	2.49	0.04	98.37	0.04	0.00
	74.38	0.29	11.94	2.43	0.09	0.22	1.54	3.07	2.52	0.01	96.49	0.04	0.00
JC12_D6_112-113_T	74.67	0.09	11.69	0.88	0.00	0.00	0.40	3.22	4.27	0.00	95.21	0.13	0.00
1158.5 cm	74.49	0.13	12.05	1.15	0.07	0.03	0.47	2.97	3.75	0.01	95.12	0.13	0.00
Hässeldalen	73.24	0.10	11.83	1.13	0.06	0.04	0.47	2.96	4.02	0.04	93.89	0.13	0.02

Figure 1: Overview map of NE Germany and NW Poland showing the location of Lake Tiefer See (TSK) and Lake Czechowskie (JC). The red dotted line indicates the position of the southerly ice advance of the Pomeranian phase at the end of the Weichselian glaciation. Inlet map is showing the position of European volcanoes mentioned in the text (black triangles) in relation to studied sites (black stars).

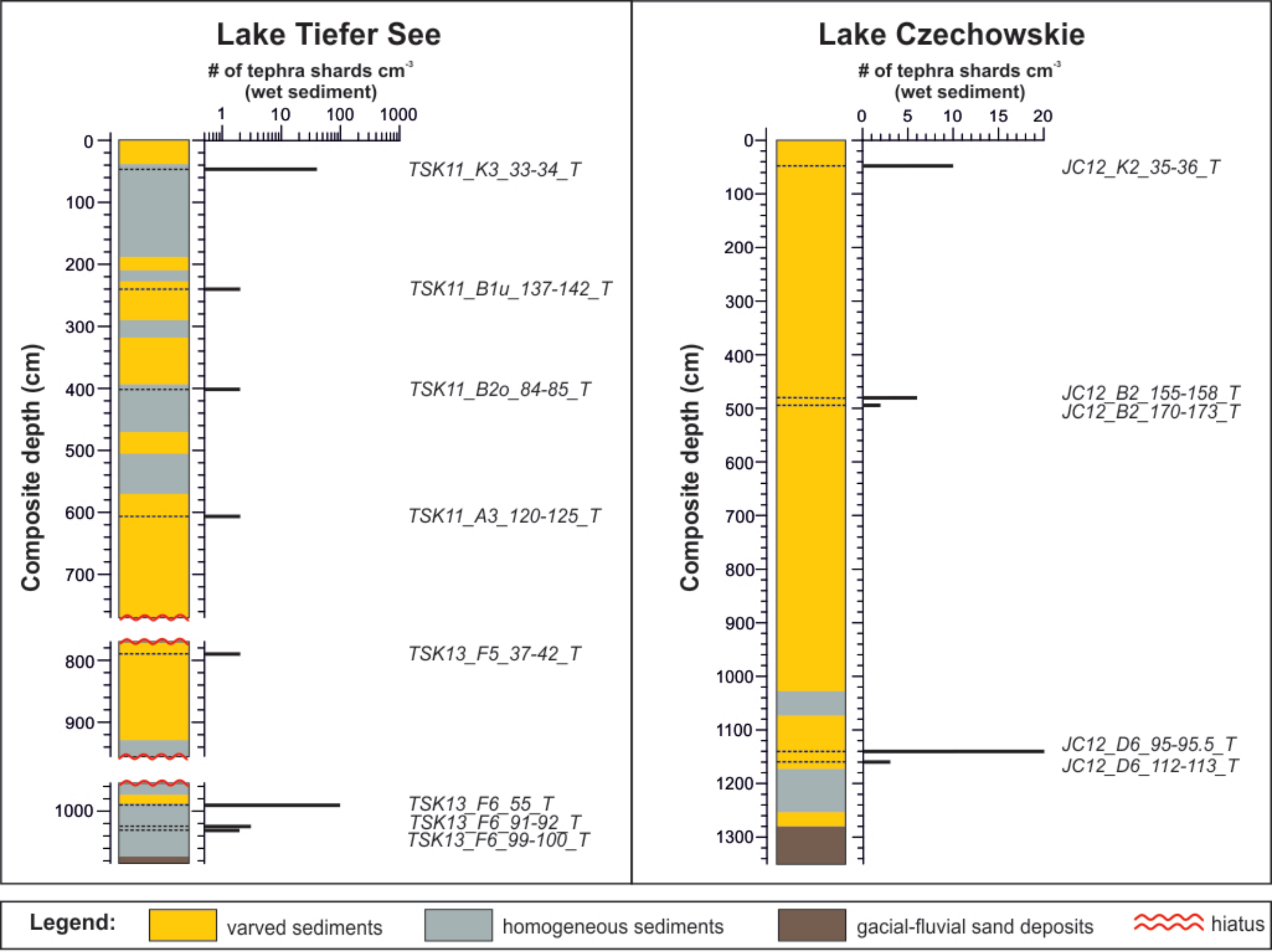

Figure 2: Lithology of the composite profile of Lake Tiefer See (left) and Lake Czechowskie (right) with positions of cryptotephras.

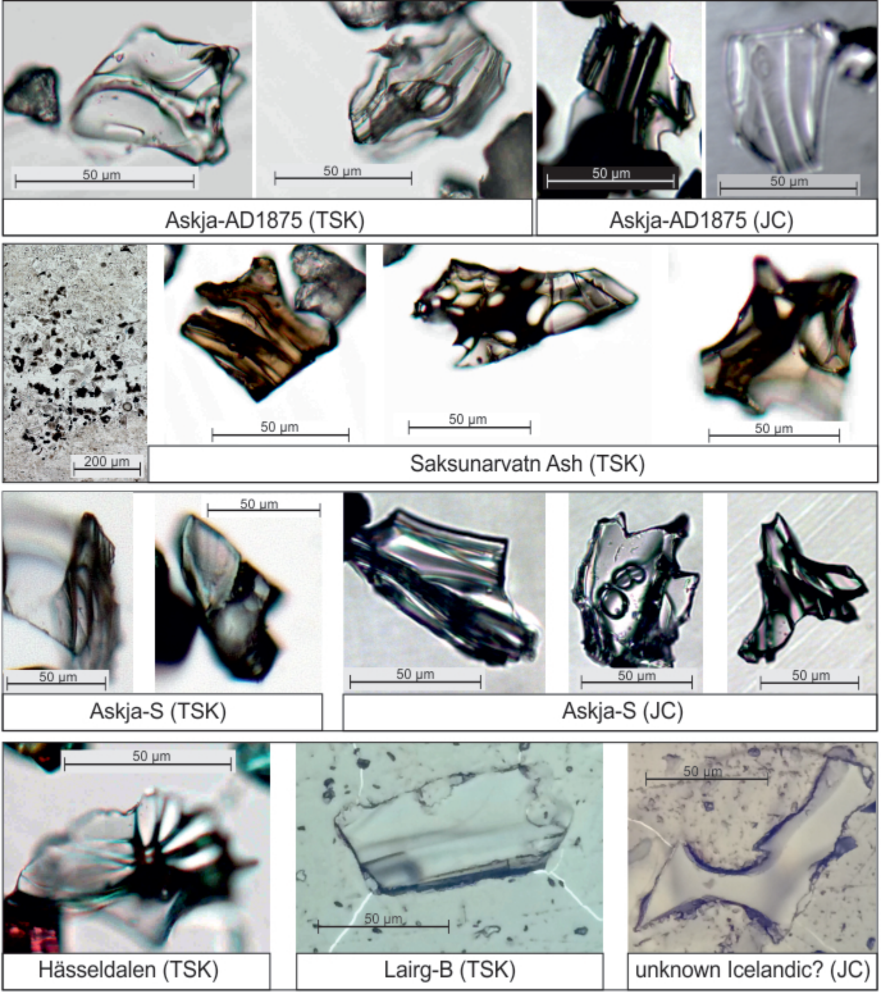

Figure 3: Transmitted light images of tephra glass shards from TSK and JC sediments correlated with Askja-AD1875 (TSK11_K3_33-34_T, JC12_K2_35-36_T), Saksunarvatn (TSK13_F6_55_T), Askja-S (TSK13_F6_91-92_T, JC12_D6_95-95.5_T), Hässeldalen (TSK13_F6_99-100_T), Lairg-B (TSK13_F5_37-42_T, polished surface) and an unknown silicic Icelandic eruption (JC09_B2_170-173_T, polished surface).

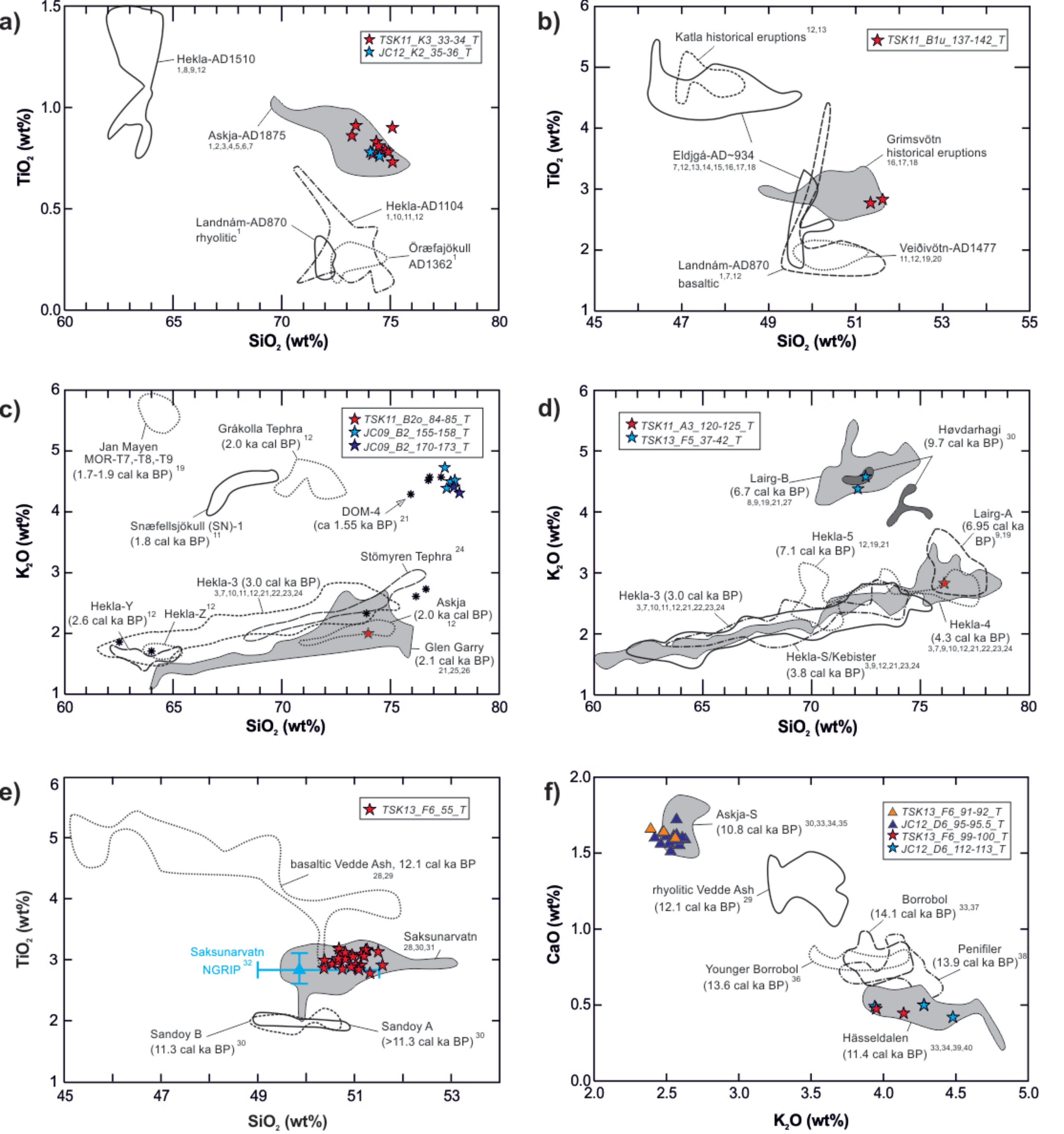

Figure 4: Geochemical bi-plots of normalized tephra glass data for tephra discrimination and correlation. (a) Askja-AD1875 tephra (TSK, JC); (b) Unknown Grimsvötn Ash (TSK); (c) Glen Garry and unknown late Holocene Icelandic tephras (TSK, JC); (d) Hekla-4 and Lairg-B tephras (TSK); (e) Saksunarvatn Ash (TSK); (f) Askja-S and Hässeldalen tephras (TSK, JC). EPMA reference data are obtained from: 1 ; 2 ; 7 this study; 8 Pilcher et al. (1996); 9 Dugmore et al. (1995b); 10 Eiríksson et al. (2000); 11 Larsen et al. (2002); 12 Óladóttir et al. (2011); 13 ; 14 ; 16 ; 19 ; 21 ; 22 Guðmundsdóttir et al. (2011); 23 Meara (2012); 24 Wastegård (2005); 25 Barber et al. (2008); 26 Housley et al. (2013); 27 Dörfler et al. (2012); 28 ; 29 ; 30 ; 31 ; 32 .; 33 ; 34 ; 35 ; 36 ; 37 ; 38 ; 39 ; 40 Lilja et al. (2013). Note that there are some effects of slight sodium migration (slightly higher SiO2 values, lower Al2O3 and Na2O concentrations) due to the small grain sizes of glass shards and respective small beam sizes that have been applied for EPMA.

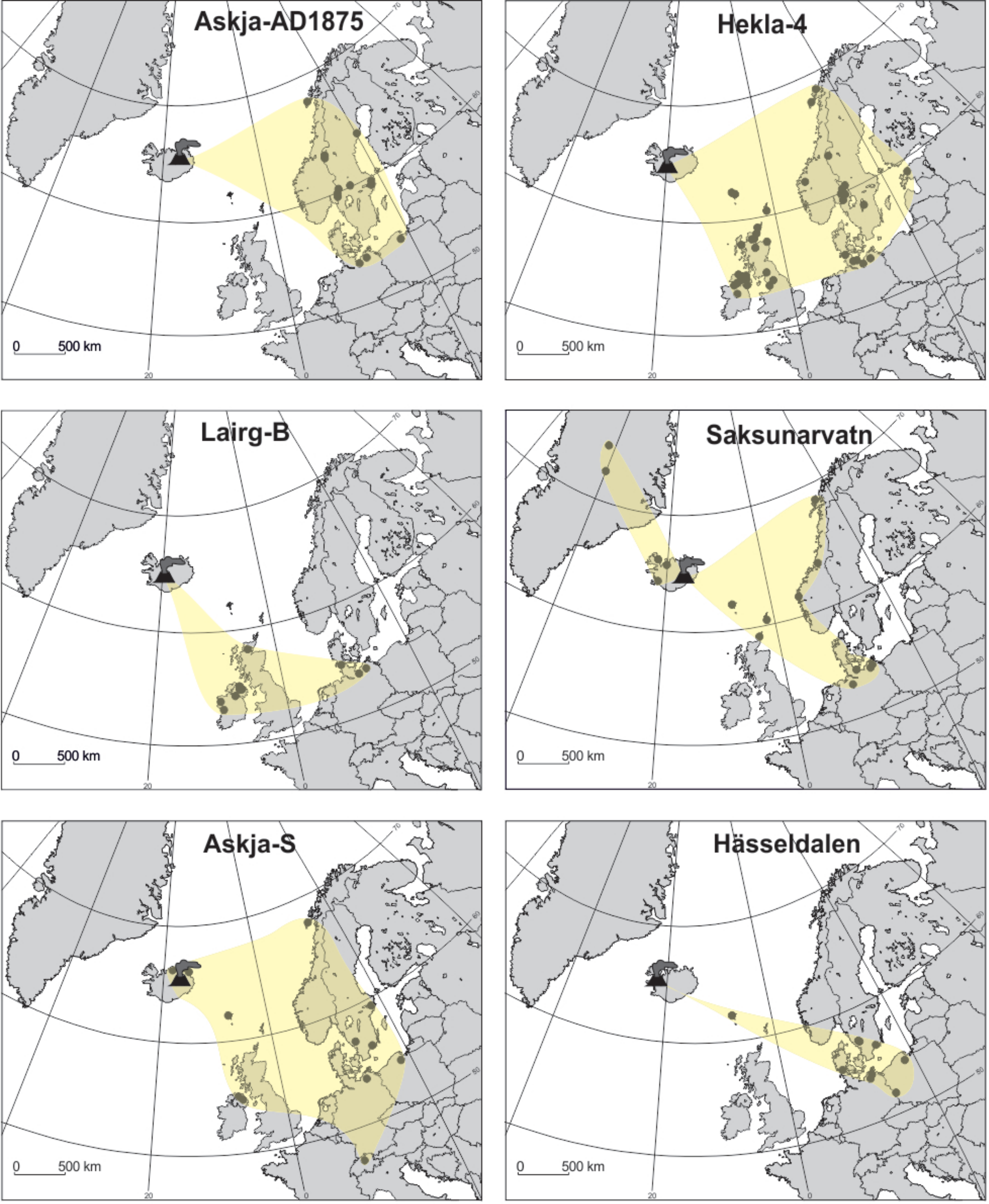

Figure 5: Dispersal maps of Holocene and Lateglacial tephras in northern-central Europe modified after Lawson et al. (2012) and Davies et al. (2012). Black filled dots represent terrestrial sites of tephra findings (references see text).

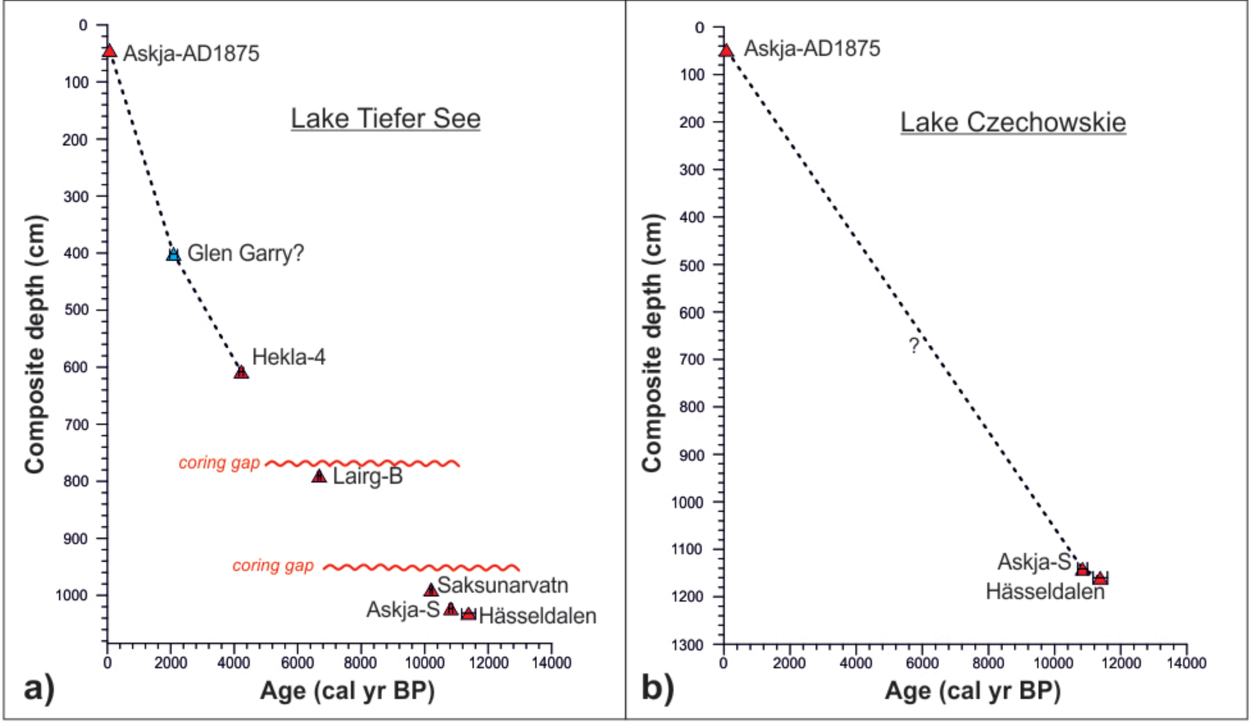

Figure 6: Tephrochronologies of sediment sequences from Lake Tiefer See (a) and Lake Czechowskie (b). Red triangles are imported tephra ages (references see text) with a 2σ error bar. The dotted lines result from linear interpolation between tephra ages, whereby the question mark at the JC tephrochronology indicates the difficulty of sedimentation rate estimations.

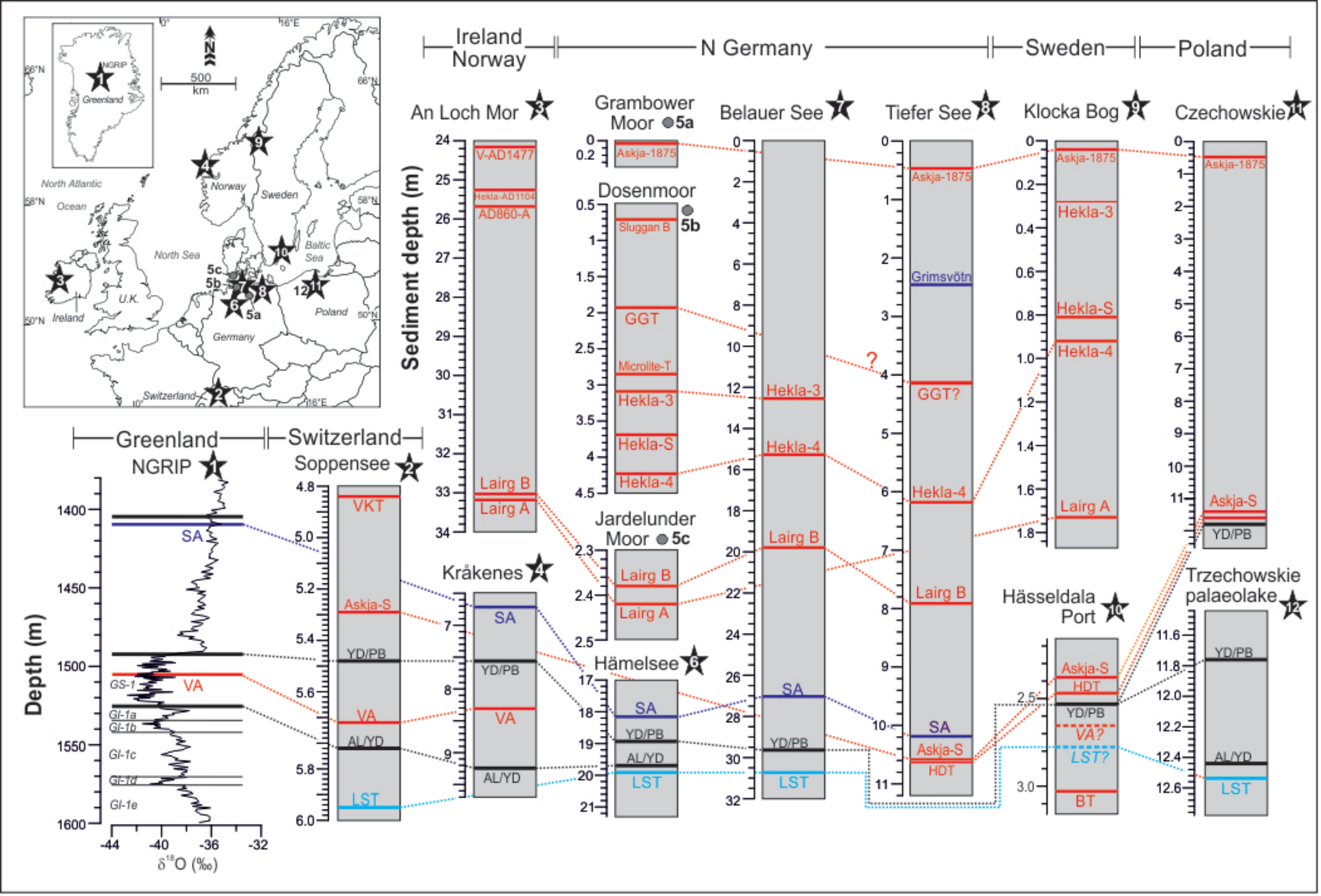

Figure 7: (a) Tephrostratigraphical linking of Lake Tiefer See and Lake Czechowskie sediment sequences with other high-resolution records from northern and central Europe. Note that all records are plotted against sediment depth in meter. Acronyms for biostratigraphical boundaries (black lines): PB=Preboreal, YD=Younger Dryas, AL=Allerød. Tephra acronyms: GGT=Glen Garry Tephra, VKT=Vasset-Kilian Tephra (French Massif Central), SA=Saksunarvatn Ash, HDT=Hässeldalen Tephra, VA=Vedde Ash, LST=Laacher See Tephra, BT=Borrobol Tephra. (b) Inlet map of central and northern Europe showing the location of sites used for tephrostratigraphical comparison. Data are obtained from: (1) NGRIP ; (2) Lake Soppensee ; (3) An Loch Mor ; (4) Kråkenes ; (5a) Grambower Moor; (5b) Dosenmoor; (5c) Jardelunder Moor ; (6) Hämelsee ; (7) Lake Belauer See ; (8) Lake Tiefer See (this study); (9) Klocka Bog ; (10) Hässeldala Port ; (11) Lake Czechowskie (this study); (12) Trzechowskie palaeolake .

Lake Tiefer See

Sample:	***TSK11_K3_33-34_T***	**Glass standard:**													
Correlation:	Askja-AD1875	Lipari obsidian	**SiO_2**	**TiO_2**	**Al_2O_3**	**FeO**	**MnO**	**MgO**	**CaO**	**Na_2O**	**K_2O**	**P_2O_5**	**Cl**	**F**	**Total**
Instrument:	JEOL JXA-8230	10 µm-beam	75.14	0.04	12.99	1.41	0.07	0.02	0.73	3.91	5.24	0.00	0.34	0.04	99.94
voltage:	15 kV	20 µm-beam	74.81	0.10	12.60	1.48	0.06	0.00	0.70	3.81	5.11	0.00	0.33	0.04	99.04
beam current:	10 nA														
beam size:	8-10 µm														

Sample:	***TSK11_B1u_137-142_T***	**Glass standard:**													
Correlation:	unknown Grimsvötn	Lipari obsidian	**SiO_2**	**TiO_2**	**Al_2O_3**	**FeO**	**MnO**	**MgO**	**CaO**	**Na_2O**	**K_2O**	**P_2O_5**	**Cl**	**F**	**Total**
Instrument:	JEOL JXA-8230	10 µm-beam	75.27	0.10	12.75	1.51	0.06	0.03	0.74	3.92	4.87	0.01	0.34	0.00	99.59
voltage:	15 kV	15 µm-beam	74.78	0.07	12.73	1.51	0.10	0.04	0.72	3.95	4.94	0.00	0.33	0.00	99.17
beam current:	10 nA	20 µm-beam	74.68	0.09	12.55	1.41	0.03	0.05	0.75	3.88	4.92	0.01	0.34	0.00	98.71
beam size:	8 µm														

Sample:	***TSK11_B2o_84-85_T***	**Glass standard:**													
Correlation:	Glen Garry?	Lipari obsidian	**SiO_2**	**TiO_2**	**Al_2O_3**	**FeO**	**MnO**	**MgO**	**CaO**	**Na_2O**	**K_2O**	**P_2O_5**	**Cl**	**F**	**Total**
Instrument:	JEOL JXA-8230	5 µm-beam	74.55	0.07	13.17	1.46	0.08	0.02	0.74	3.83	5.22	0.00	0.36	0.00	99.50
voltage:	15 kV	10 µm-beam	73.94	0.04	13.05	1.51	0.08	0.05	0.72	3.61	5.26	0.00	0.34	0.07	98.66
beam current:	10 nA	15 µm-beam	74.61	0.10	13.22	1.58	0.02	0.06	0.73	3.99	5.21	0.00	0.36	0.00	99.89
beam size:	8 µm	20 µm-beam	74.41	0.09	12.99	1.51	0.06	0.03	0.73	3.79	5.15	0.00	0.38	0.00	99.14

Sample:	***TSK11_A3_120-125_T***	**Glass standard:**													
Correlation:	Hekla-4	Lipari obsidian	**SiO_2**	**TiO_2**	**Al_2O_3**	**FeO**	**MnO**	**MgO**	**CaO**	**Na_2O**	**K_2O**	**P_2O_5**	**Cl**	**F**	**Total**
Instrument:	JEOL JXA-8230	5 µm-beam	74.55	0.07	13.17	1.46	0.08	0.02	0.74	3.83	5.22	0.00	0.36	0.00	99.50
voltage:	15 kV	10 µm-beam	73.94	0.04	13.05	1.51	0.08	0.05	0.72	3.61	5.26	0.00	0.34	0.07	98.66
beam current:	10 nA	15 µm-beam	74.61	0.10	13.22	1.58	0.02	0.06	0.73	3.99	5.21	0.00	0.36	0.00	99.89
beam size:	5 µm	20 µm-beam	74.41	0.09	12.99	1.51	0.06	0.03	0.73	3.79	5.15	0.00	0.38	0.00	99.14

Sample:	***TSK13_F5_37-43_T***	**Glass standard:**

Correlation:	Lairg-B	Lipari obsidian	**SiO_2**	**TiO_2**	**Al_2O_3**	**FeO**	**MnO**	**MgO**	**CaO**	**Na_2O**	**K_2O**	**P_2O_5**	**Cl**	**F**	**Total**
Instrument:	JEOL JXA-8230	5 µm-beam	73.46	0.08	13.27	1.42	0.08	0.05	0.64	4.01	5.19	0.00	0.35	0.00	98.55
voltage:	15 kV	10 µm-beam	73.34	0.06	13.33	1.44	0.03	0.05	0.62	4.31	5.11	0.03	0.35	0.00	98.66
beam current:	10 nA	20 µm-beam	72.79	0.09	13.16	1.39	0.11	0.05	0.57	4.39	5.02	0.00	0.38	0.00	97.95
beam size:	8 µm														

Sample:	***TSK13_F6_55_T***	**Glass standard:**													
Correlation:	Saksunarvatn	Lipari obsidian	**SiO_2**	**TiO_2**	**Al_2O_3**	**FeO**	**MnO**	**MgO**	**CaO**	**Na_2O**	**K_2O**	**P_2O_5**	**Cl**	**F**	**Total**
Instrument:	JEOL JXA-8230	10 µm-beam	76.08	0.12	12.81	1.53	0.07	0.05	0.73	3.83	5.04	0.03	0.33	0.00	100.62
voltage:	15 kV	20 µm-beam	75.36	0.07	12.64	1.48	0.08	0.03	0.76	3.96	5.24	0.00	0.33	0.03	99.98
beam current:	10 nA														
beam size:	10 µm														

Sample:	***TSK13_F6_91-92_T***	**Glass standard:**													
Correlation:	Askja-S	Lipari obsidian	**SiO_2**	**TiO_2**	**Al_2O_3**	**FeO**	**MnO**	**MgO**	**CaO**	**Na_2O**	**K_2O**	**P_2O_5**	**Cl**	**F**	**Total**
Instrument:	JEOL JXA-8230	5 µm-beam	74.14	0.10	13.04	2.03	0.11	0.03	0.71	3.80	5.12	0.00	0.31	0.00	99.39
voltage:	15 kV	10 µm-beam	74.58	0.07	13.20	1.66	0.07	0.07	0.78	3.91	5.23	0.01	0.33	0.00	99.90
beam current:	10 nA	15 µm-beam	74.81	0.09	13.02	1.55	0.03	0.02	0.74	4.10	5.30	0.02	0.37	0.00	100.06
beam size:	5 µm	20 µm-beam	74.95	0.09	13.17	1.57	0.08	0.04	0.71	3.88	5.15	0.00	0.35	0.00	99.99

Sample:	***TSK13_F6_99-100_T***	**Glass standard:**													
Correlation:	Hässeldalen	Lipari obsidian	**SiO_2**	**TiO_2**	**Al_2O_3**	**FeO**	**MnO**	**MgO**	**CaO**	**Na_2O**	**K_2O**	**P_2O_5**	**Cl**	**F**	**Total**
Instrument:	JEOL JXA-8230	10 µm-beam	76.06	0.07	12.95	1.45	0.06	0.06	0.72	3.73	5.07	0.00	0.35	0.02	100.53
voltage:	15 kV	15 µm-beam	75.96	0.11	12.87	1.52	0.05	0.04	0.76	3.79	5.17	0.01	0.38	0.00	100.66
beam current:	10 nA	20 µm-beam	75.78	0.03	12.80	1.63	0.05	0.04	0.71	3.90	5.16	0.02	0.33	0.00	100.45
beam size:	8 µm														

Lake Czechowskie

Sample:	***JC12_K2_35-36_T***	**Glass standard:**													
Correlation:	Askja-AD1875	Lipari obsidian	**SiO_2**	**TiO_2**	**Al_2O_3**	**FeO**	**MnO**	**MgO**	**CaO**	**Na_2O**	**K_2O**	**P_2O_5**	**Cl**	**F**	**Total**
Instrument:	JEOL JXA-8230	10 µm-beam	76.06	0.07	12.95	1.45	0.06	0.06	0.72	3.73	5.07	0.00	0.35	0.02	100.53
voltage:	15 kV	15 µm-beam	75.96	0.11	12.87	1.52	0.05	0.04	0.76	3.79	5.17	0.01	0.38	0.00	100.66
beam current:	10 nA	20 µm-beam	75.78	0.03	12.80	1.63	0.05	0.04	0.71	3.90	5.16	0.02	0.33	0.00	100.45
beam size:	8 µm														

Sample:	***JC09_B2_155-158_T***	**Glass standard:**													
	JC09_B2_170-173_T	Lipari obsidian	**SiO_2**	**TiO_2**	**Al_2O_3**	**FeO**	**MnO**	**MgO**	**CaO**	**Na_2O**	**K_2O**	**P_2O_5**	**Cl**	**F**	**Total**
Correlation:	?	5 µm-beam	73.46	0.08	13.27	1.42	0.08	0.05	0.64	4.01	5.19	0.00	0.35	0.00	98.55
Instrument:	JEOL JXA-8230	10 µm-beam	73.34	0.06	13.33	1.44	0.03	0.05	0.62	4.31	5.11	0.03	0.35	0.00	98.66
voltage:	15 kV	20 µm-beam	72.79	0.09	13.16	1.39	0.11	0.05	0.57	4.39	5.02	0.00	0.38	0.00	97.95
beam current:	10 nA														
beam size:	8 µm														

Sample:	***JC12_D6_95-95.5_T***	**Glass standard:**													
Correlation:	Askja-S	Lipari obsidian	**SiO_2**	**TiO_2**	**Al_2O_3**	**FeO**	**MnO**	**MgO**	**CaO**	**Na_2O**	**K_2O**	**P_2O_5**	**Cl**	**F**	**Total**
Instrument:	JEOL JXA-8230	10 µm-beam	73.61	0.09	12.87	1.55	0.06	0.03	0.71	4.02	5.22	0.02	0.37	0.00	98.55
voltage:	15 kV	15 µm-beam	73.53	0.10	12.85	1.61	0.11	0.02	0.72	4.06	5.30	0.00	0.37	0.00	98.66
beam current:	10 nA	20 µm-beam	73.56	0.05	12.78	1.49	0.11	0.05	0.72	4.01	5.26	0.00	0.34	0.00	98.36
beam size:	5-8 µm														

Sample:	***JC12_D6_112-113_T***	**Glass standard:**													
Correlation:	Hässeldalen	Lipari obsidian	**SiO_2**	**TiO_2**	**Al_2O_3**	**FeO**	**MnO**	**MgO**	**CaO**	**Na_2O**	**K_2O**	**P_2O_5**	**Cl**	**F**	**Total**
Instrument:	JEOL JXA-8230	5 µm-beam	74.14	0.10	13.04	2.03	0.11	0.03	0.71	3.80	5.12	0.00	0.31	0.00	99.39
voltage:	15 kV	10 µm-beam	74.58	0.07	13.20	1.66	0.07	0.07	0.78	3.91	5.23	0.01	0.33	0.00	99.90
beam current:	10 nA	15 µm-beam	74.81	0.09	13.02	1.55	0.03	0.02	0.74	4.10	5.30	0.02	0.37	0.00	100.06
beam size:	5 µm	20 µm-beam	74.95	0.09	13.17	1.57	0.08	0.04	0.71	3.88	5.15	0.00	0.35	0.00	99.99

Proximal Icelandic Tephras

Sample	Beam size	SiO_2	TiO_2	Al_2O_3	FeO	MnO	MgO	CaO	Na_2O	K_2O	P_2O_5	Cl	F	Total	Origin
Askja-AD1875 proximal	5 µm	74.25	0.81	12.92	3.76	0.10	0.69	2.31	3.38	2.46	0.12	0.04	0.00	100.85	proximal deposits of Unit D of the Askja-AD1875 eruption
Askja-AD1875 proximal	5 µm	73.61	0.78	12.75	3.52	0.10	0.68	2.22	3.29	2.50	0.17	0.04	0.00	99.67	Location: section at Herdubreidatögl, 20 km ENE (60°) of Askja
Askja-AD1875 proximal	5 µm	74.73	0.72	12.58	3.42	0.13	0.55	2.02	3.28	2.55	0.08	0.05	0.00	100.10	
Askja-AD1875 proximal	5 µm	73.94	0.80	12.59	3.72	0.08	0.63	2.19	3.43	2.46	0.14	0.05	0.00	100.02	
Askja-AD1875 proximal	5 µm	73.80	0.73	12.73	3.45	0.12	0.70	2.35	3.37	2.53	0.18	0.04	0.00	99.99	
Askja-AD1875 proximal	5 µm	74.98	0.75	12.50	3.69	0.07	0.47	1.95	3.69	2.63	0.12	0.05	0.00	100.90	
Askja-AD1875 proximal	5 µm	73.44	0.84	12.92	3.76	0.08	0.73	2.36	3.65	2.41	0.14	0.05	0.02	100.39	
Askja-AD1875 proximal	5 µm	74.34	0.80	12.76	3.59	0.07	0.65	2.30	3.41	2.53	0.15	0.03	0.00	100.63	
Askja-AD1875 proximal	5 µm	73.73	0.77	12.67	3.58	0.11	0.65	2.28	3.70	2.51	0.09	0.05	0.06	100.19	
Askja-AD1875 proximal	5 µm	73.02	0.79	13.02	3.99	0.10	0.75	2.57	3.33	2.30	0.20	0.05	0.00	100.11	
Askja-AD1875 proximal	5 µm	73.59	0.81	12.89	4.01	0.13	0.77	2.50	3.59	2.38	0.09	0.05	0.01	100.82	
Askja-AD1875 proximal	5 µm	73.50	0.80	12.90	3.62	0.12	0.65	2.31	3.69	2.37	0.15	0.06	0.00	100.18	
Askja-AD1875 proximal	5 µm	73.30	0.72	13.02	3.50	0.11	0.65	2.35	3.65	2.43	0.17	0.04	0.02	99.96	
Askja-AD1875 proximal	5 µm	72.67	0.81	12.74	3.85	0.08	0.70	2.31	3.43	2.31	0.16	0.05	0.00	99.11	
Askja-AD1875 proximal	5 µm	71.62	0.96	13.13	4.60	0.09	0.85	2.93	3.71	2.17	0.22	0.04	0.01	100.33	
Askja-AD1875 proximal	5 µm	73.40	0.82	12.98	3.77	0.09	0.72	2.29	3.27	2.38	0.18	0.05	0.03	99.98	
Askja-AD1875 proximal	5 µm	73.92	0.74	12.71	3.39	0.11	0.61	2.06	3.28	2.50	0.19	0.04	0.00	99.54	
Askja-AD1875 proximal	5 µm	73.34	0.92	12.97	4.01	0.10	0.81	2.43	3.25	2.42	0.17	0.04	0.00	100.46	
Askja-AD1875 proximal	5 µm	73.41	0.81	12.79	3.49	0.06	0.68	2.21	3.46	2.42	0.11	0.04	0.02	99.52	
Askja-AD1875 proximal	5 µm	74.56	0.72	12.45	3.20	0.08	0.49	2.00	3.22	2.56	0.09	0.04	0.00	99.41	
Askja-AD1875 proximal	5 µm	72.55	0.86	13.27	4.08	0.14	0.81	2.66	3.45	2.31	0.16	0.04	0.02	100.34	
Askja-AD1875 proximal	5 µm	73.83	0.78	12.91	3.67	0.11	0.66	2.29	3.54	2.48	0.19	0.05	0.00	100.50	
Askja-AD1875 proximal	5 µm	73.37	0.84	12.71	3.83	0.09	0.70	2.27	3.40	2.38	0.17	0.04	0.00	99.80	
Askja-AD1875 proximal	5 µm	73.93	0.78	12.65	3.61	0.09	0.63	2.27	3.63	2.52	0.14	0.05	0.00	100.29	
Landnám-AD870	8 µm	50.79	1.76	13.55	12.51	0.23	7.02	11.36	2.40	0.21	0.15	0.02	0.00	99.99	medial-dital deposits of the Landnám-AD870 eruption
Landnám-AD870	8 µm	50.31	1.73	13.41	13.01	0.19	7.14	11.43	2.35	0.22	0.19	0.01	0.01	100.00	Location: road cut on Road F26 (Sigalda)
Landnám-AD870	8 µm	50.56	1.70	13.27	11.40	0.20	6.96	11.40	2.31	0.17	0.18	0.01	0.00	98.17	

Landnám-AD870	8 µm	50.79	1.86	13.33	13.13	0.26	6.82	11.09	2.35	0.24	0.17	0.02	0.00	100.05	
Landnám-AD870	8 µm	50.58	1.77	13.18	11.73	0.19	7.05	11.37	2.38	0.24	0.18	0.01	0.00	98.67	
Landnám-AD870	8 µm	50.19	1.70	13.43	12.43	0.21	7.03	11.32	2.32	0.21	0.16	0.02	0.00	99.03	
Landnám-AD870	8 µm	51.10	1.83	13.40	12.51	0.19	6.57	11.17	2.47	0.21	0.21	0.00	0.00	99.66	
Landnám-AD870	8 µm	50.79	1.90	13.45	12.22	0.20	6.99	11.39	2.41	0.21	0.17	0.00	0.00	99.73	
Landnám-AD870	8 µm	50.18	1.76	13.41	12.38	0.22	6.90	11.36	2.25	0.24	0.20	0.00	0.00	98.90	
Landnám-AD870	8 µm	50.54	1.78	13.48	11.96	0.21	7.03	11.38	2.29	0.17	0.14	0.01	0.00	98.99	
Landnám-AD870	8 µm	50.58	1.91	13.14	12.66	0.22	6.70	11.05	2.45	0.23	0.20	0.01	0.00	99.15	
Landnám-AD870	8 µm	50.65	1.89	13.34	12.52	0.18	6.73	11.10	2.38	0.23	0.21	0.01	0.00	99.24	
Landnám-AD870	8 µm	50.82	1.96	13.18	13.57	0.25	6.69	10.99	2.36	0.21	0.21	0.01	0.00	100.25	
Landnám-AD870	8 µm	50.51	1.84	13.18	11.99	0.22	6.96	11.40	2.39	0.22	0.18	0.02	0.00	98.91	
Landnám-AD870	8 µm	50.57	1.83	13.28	13.13	0.23	6.67	11.05	2.42	0.22	0.20	0.01	0.00	99.61	
Landnám-AD870	8 µm	50.34	1.68	13.31	12.01	0.19	6.97	11.37	2.34	0.23	0.23	0.00	0.00	98.68	
Landnám-AD870	8 µm	49.96	1.78	13.07	11.81	0.19	6.98	11.39	2.22	0.20	0.17	0.01	0.02	97.80	
Landnám-AD870	10 µm	48.66	1.83	13.40	12.47	0.25	7.05	11.55	2.40	0.21	0.15	0.02	0.00	97.99	proximal deposits of the Landnám-AD870 eruption
Landnám-AD870	10 µm	50.03	1.67	13.42	12.06	0.20	7.11	11.67	2.43	0.20	0.17	0.00	0.00	98.96	Location: Vatnaöldur tephra ring
Landnám-AD870	10 µm	50.64	1.72	13.79	12.97	0.24	6.81	11.67	2.37	0.18	0.20	0.01	0.00	100.60	
Landnám-AD870	10 µm	50.18	1.81	13.54	12.52	0.27	7.10	11.58	2.46	0.23	0.16	0.01	0.00	99.86	
Landnám-AD870	10 µm	50.61	1.87	13.62	12.35	0.19	7.09	11.51	2.39	0.22	0.19	0.01	0.00	100.05	
Landnám-AD870	10 µm	51.31	1.75	13.63	12.44	0.25	7.04	11.53	2.41	0.24	0.21	0.01	0.00	100.83	
Landnám-AD870	10 µm	50.80	1.83	13.78	12.44	0.26	6.99	11.68	1.89	0.27	0.17	0.01	0.00	100.12	
Landnám-AD870	10 µm	49.55	1.83	13.65	12.34	0.22	7.12	11.55	2.50	0.23	0.15	0.00	0.00	99.14	
Landnám-AD870	10 µm	49.93	1.82	13.46	12.83	0.18	7.00	11.33	2.53	0.25	0.20	0.00	0.00	99.53	
Landnám-AD870	10 µm	50.20	1.82	13.86	12.60	0.25	7.18	11.53	2.30	0.26	0.18	0.02	0.00	100.20	
Landnám-AD870	10 µm	50.51	1.77	13.69	12.51	0.24	7.07	11.60	2.38	0.22	0.16	0.00	0.00	100.16	
Landnám-AD870	10 µm	50.73	1.85	13.76	12.37	0.22	7.16	11.57	1.92	0.17	0.16	0.01	0.00	99.92	
Landnám-AD870	10 µm	50.94	1.90	13.82	11.72	0.26	6.78	11.25	2.20	0.26	0.20	0.02	0.00	99.35	
Landnám-AD870	10 µm	50.71	1.79	13.57	12.49	0.26	7.07	11.41	2.51	0.25	0.19	0.01	0.00	100.26	
Landnám-AD870	10 µm	51.05	1.74	13.70	12.39	0.25	7.02	11.62	1.65	0.20	0.17	0.01	0.00	99.81	
Landnám-AD870	10 µm	50.28	1.73	13.53	12.37	0.21	7.04	11.49	2.27	0.22	0.16	0.01	0.00	99.31	

Landnám-AD870	10 µm	50.28	1.81	13.42	12.55	0.20	7.16	11.56	2.37	0.20	0.14	0.01	0.00	99.70	
Landnám-AD870	10 µm	50.80	1.78	13.60	12.13	0.18	6.78	11.54	2.47	0.21	0.17	0.00	0.00	99.66	
Landnám-AD870	10 µm	50.57	1.82	13.68	12.47	0.22	7.18	11.52	2.22	0.25	0.17	0.01	0.00	100.11	
Landnám-AD870	10 µm	50.54	1.82	13.58	12.45	0.23	7.06	11.48	2.45	0.22	0.18	0.01	0.00	100.01	
Landnám-AD870	10 µm	50.11	1.80	13.67	12.75	0.24	6.95	11.76	2.43	0.21	0.17	0.01	0.00	100.10	
Landnám-AD870	10 µm	50.26	1.76	13.60	12.46	0.24	7.05	11.44	2.43	0.25	0.17	0.01	0.00	99.67	
Landnám-AD870	10 µm	50.17	1.81	13.40	12.87	0.27	7.12	11.30	2.49	0.25	0.21	0.01	0.00	99.89	
Landnám-AD870	10 µm	50.28	1.84	13.29	12.59	0.29	6.74	11.37	2.41	0.20	0.17	0.00	0.00	99.18	
Landnám-AD870	10 µm	50.44	1.76	13.63	12.66	0.23	7.07	11.59	2.28	0.21	0.15	0.00	0.00	100.02	
Landnám-AD870	10 µm	49.77	1.91	13.43	12.35	0.25	7.15	11.54	2.39	0.21	0.13	0.00	0.00	99.14	
Landnám-AD870	10 µm	50.55	1.72	13.63	12.38	0.23	7.06	11.55	2.32	0.21	0.18	0.00	0.00	99.84	
Landnám-AD870	10 µm	50.26	1.78	13.24	12.17	0.24	6.97	11.59	2.39	0.23	0.19	0.00	0.00	99.05	
Eldgjá-AD~934	8 µm	48.25	4.64	12.29	14.33	0.24	5.21	9.67	3.01	0.77	0.60	0.05	0.00	99.06	medial-distal deposits of the Eldgjá-AD~934 eruption
Eldgjá-AD~934	8 µm	47.90	4.73	12.42	15.57	0.19	4.91	9.21	3.15	0.92	0.55	0.04	0.00	99.59	Location: east of Myrdalsjökull, ca 15 km east of eruption site
Eldgjá-AD~934	8 µm	48.32	4.63	12.38	15.13	0.26	5.14	9.42	3.00	0.78	0.56	0.00	0.00	99.61	
Eldgjá-AD~934	8 µm	48.38	4.61	12.32	15.05	0.25	5.16	9.41	3.01	0.73	0.56	0.03	0.00	99.50	
Eldgjá-AD~934	8 µm	47.75	4.75	12.18	14.89	0.23	5.34	9.42	2.91	0.85	0.59	0.04	0.00	98.94	
Eldgjá-AD~934	8 µm	48.35	4.50	12.22	14.63	0.19	5.30	9.51	3.00	0.72	0.57	0.03	0.00	99.02	
Eldgjá-AD~934	8 µm	47.89	4.60	12.17	14.38	0.22	5.24	9.66	2.89	0.75	0.48	0.04	0.00	98.31	
Eldgjá-AD~934	8 µm	48.17	4.62	12.51	15.56	0.16	5.23	9.59	3.02	0.69	0.60	0.02	0.00	100.18	
Eldgjá-AD~934	8 µm	48.18	4.44	12.52	14.08	0.21	5.03	9.45	3.05	0.77	0.64	0.02	0.00	98.39	
Eldgjá-AD~934	8 µm	47.86	4.59	12.27	15.23	0.24	4.85	9.41	3.09	0.81	0.63	0.04	0.03	99.05	
Eldgjá-AD~934	8 µm	48.03	4.74	12.27	15.65	0.19	5.20	9.61	2.84	0.74	0.60	0.04	0.00	99.90	
Eldgjá-AD~934	8 µm	49.07	4.46	12.53	14.03	0.22	4.69	9.22	3.14	0.83	0.67	0.03	0.00	98.88	
Eldgjá-AD~934	8 µm	46.66	5.37	12.22	17.67	0.22	5.12	8.92	3.06	0.72	0.53	0.03	0.00	100.51	
Eldgjá-AD~934	8 µm	48.29	4.53	12.36	15.59	0.26	5.34	9.48	2.82	0.72	0.58	0.03	0.00	100.00	
Eldgjá-AD~934	8 µm	48.10	4.82	11.40	15.97	0.28	4.79	9.40	3.03	0.97	0.77	0.04	0.00	99.57	
Eldgjá-AD~934	8 µm	48.03	4.75	11.80	15.53	0.24	5.17	9.28	2.84	0.76	0.58	0.04	0.08	99.10	
Eldgjá-AD~934	8 µm	48.14	4.79	11.65	15.90	0.23	5.22	9.36	2.76	0.77	0.59	0.04	0.00	99.45	
Eldgjá-AD~934	8 µm	48.34	4.60	12.45	15.60	0.30	5.16	9.44	3.12	0.75	0.56	0.03	0.00	100.35	

Eldgjá-AD~934	8 µm	47.73	4.70	12.26	15.01	0.20	5.13	9.30	3.06	0.71	0.58	0.03	0.00	98.71	
Eldgjá-AD~934	8 µm	47.57	4.58	12.01	14.89	0.23	5.46	9.49	3.16	0.77	0.56	0.03	0.00	98.75	
Eldgjá-AD~934	8 µm	48.12	4.66	12.40	15.08	0.28	5.17	9.46	3.05	0.71	0.60	0.05	0.00	99.57	
Hekla 3	5 µm	73.97	0.26	13.93	0.13	2.94	0.09	2.01	3.47	2.44	0.01	0.06	0.00	99.30	white pumices of proximal deposits of the Hekla-3 eruption
Hekla 3	5 µm	72.78	0.16	13.48	0.12	2.89	0.11	1.94	2.81	2.34	0.04	0.05	0.13	96.85	Location: Trjávidarlœkur gully, 15 km WSW of Hekla volcano
Hekla 3	5 µm	73.84	0.26	14.23	0.15	3.67	0.15	2.32	3.57	2.43	0.03	0.04	0.00	100.70	
Hekla 3	5 µm	68.97	0.36	14.23	0.15	4.85	0.25	2.91	2.99	2.16	0.07	0.08	0.00	97.03	
Hekla 3	5 µm	71.67	0.34	14.55	0.17	5.09	0.28	3.06	3.51	2.13	0.07	0.06	0.03	100.94	
Hekla 3	5 µm	69.17	0.29	14.32	0.15	4.72	0.23	2.84	3.30	2.23	0.08	0.05	0.03	97.42	
Hekla 3	5 µm	70.33	0.33	14.56	0.15	4.94	0.30	3.22	3.37	2.13	0.03	0.05	0.00	99.41	
Hekla 3	5 µm	71.03	0.34	14.85	0.18	5.02	0.24	3.28	3.24	2.14	0.06	0.05	0.00	100.44	
Hekla 3	5 µm	68.54	0.41	14.96	0.17	5.68	0.43	3.25	3.68	2.07	0.08	0.05	0.00	99.32	
Hekla 3	5 µm	73.86	0.26	14.08	0.09	3.05	0.14	2.13	3.12	2.54	0.01	0.07	0.00	99.35	
Hekla 3	5 µm	70.22	0.29	14.69	0.17	4.88	0.31	3.01	3.69	2.12	0.03	0.05	0.00	99.46	
Hekla 3	5 µm	71.28	0.26	14.08	0.17	4.03	0.26	2.54	3.19	2.29	0.04	0.06	0.00	98.19	
Hekla 3	5 µm	74.39	0.23	14.16	0.09	2.97	0.15	2.05	3.29	2.57	0.02	0.06	0.00	99.98	
Hekla 3	5 µm	71.79	0.24	14.48	0.14	4.12	0.20	2.76	3.56	2.39	0.03	0.05	0.00	99.76	
Hekla 3	5 µm	71.32	0.20	13.53	0.13	2.93	0.11	1.97	3.24	2.43	0.01	0.06	0.04	95.97	
Hekla 3	5 µm	71.28	0.23	14.31	0.13	4.02	0.20	2.72	3.24	2.26	0.04	0.05	0.00	98.48	
Hekla 3	5 µm	71.44	0.37	14.95	0.16	4.91	0.31	2.98	3.56	2.13	0.04	0.04	0.00	100.89	
Hekla 3	5 µm	68.43	0.27	14.28	0.17	4.54	0.30	2.75	3.33	2.26	0.06	0.05	0.00	96.45	
Hekla 3	5 µm	70.63	0.25	14.34	0.15	3.94	0.16	2.53	3.02	2.12	0.04	0.07	0.01	97.25	
Hekla 4	5 µm	76.14	0.09	13.21	1.97	0.10	0.01	1.37	3.63	2.77	0.01	0.05	0.10	99.45	white pumices of proximal deposits of the Hekla-4 eruption
Hekla 4	5 µm	76.41	0.16	13.27	1.95	0.09	0.01	1.34	3.55	2.69	0.00	0.06	0.06	99.58	Location: Trjávidarlœkur gully, 15 km WSW of Hekla volcano
Hekla 4	5 µm	75.97	0.11	12.92	1.92	0.11	0.02	1.34	3.63	2.84	0.01	0.05	0.16	99.08	
Hekla 4	5 µm	75.03	0.07	12.80	1.91	0.06	0.01	1.31	3.46	2.85	0.02	0.05	0.06	97.64	
Hekla 4	5 µm	76.71	0.12	13.24	1.98	0.09	0.00	1.31	3.57	2.83	0.00	0.07	0.09	100.00	
Hekla 4	5 µm	76.15	0.08	13.30	1.85	0.07	0.02	1.26	2.88	2.58	0.02	0.06	0.00	98.28	
Hekla 4	5 µm	75.15	0.20	12.86	1.89	0.09	0.01	1.35	3.60	2.82	0.01	0.05	0.02	98.05	
Hekla 4	5 µm	76.60	0.12	12.70	1.85	0.07	0.01	1.28	3.32	2.82	0.02	0.07	0.00	98.86	

Hekla 4	5 µm	75.88	0.06	12.96	1.86	0.09	0.04	1.29	3.20	2.85	0.01	0.07	0.01	98.30
Hekla 4	5 µm	76.38	0.10	12.99	1.89	0.08	0.03	1.31	3.53	2.90	0.01	0.05	0.13	99.41
Hekla 4	5 µm	75.98	0.11	13.08	1.97	0.07	0.05	1.33	3.77	2.74	0.01	0.07	0.11	99.29
Hekla 4	5 µm	73.77	0.11	12.70	1.88	0.05	0.03	1.30	3.35	2.75	0.02	0.07	0.00	96.03
Hekla 4	5 µm	75.99	0.10	12.90	2.02	0.11	0.02	1.36	3.56	2.82	0.00	0.05	0.00	98.95
Hekla 4	5 µm	76.32	0.05	13.17	1.98	0.09	0.04	1.35	3.58	2.63	0.01	0.07	0.09	99.37
Hekla 4	5 µm	76.13	0.11	13.01	1.96	0.07	0.04	1.29	3.49	2.80	0.00	0.06	0.00	98.96
Hekla 4	5 µm	75.99	0.11	13.08	1.98	0.07	0.01	1.32	3.41	2.82	0.04	0.06	0.03	98.90
Hekla 4	5 µm	76.38	0.12	13.01	1.95	0.04	0.06	1.36	3.69	2.84	0.03	0.05	0.05	99.59
Hekla 4	5 µm	76.42	0.11	13.03	1.93	0.11	0.00	1.32	3.58	2.83	0.00	0.05	0.00	99.40
Hekla 4	5 µm	75.96	0.08	13.13	1.92	0.10	0.00	1.30	3.49	2.76	0.02	0.05	0.09	98.91
Hekla 4	5 µm	75.56	0.12	12.99	2.04	0.12	0.02	1.31	3.70	2.77	0.02	0.06	0.07	98.79
Hekla 4	5 µm	76.68	0.08	13.18	1.88	0.06	0.00	1.36	3.64	2.83	0.02	0.07	0.00	99.81
Hekla 4	5 µm	75.18	0.09	12.94	1.90	0.05	0.01	1.33	3.48	2.74	0.00	0.05	0.00	97.77
Hekla 4	5 µm	76.87	0.12	13.17	1.92	0.09	0.06	1.32	3.58	2.77	0.00	0.05	0.04	99.98
Hekla 4	5 µm	76.65	0.18	13.11	1.97	0.08	0.03	1.33	3.52	2.69	0.02	0.07	0.10	99.75
Hekla 4	5 µm	75.65	0.08	13.02	1.87	0.08	0.03	1.29	3.26	2.81	0.00	0.06	0.02	98.18

Secondary glass standard	**Beam size**	**SiO_2**	**TiO_2**	**Al_2O_3**	**FeO**	**MnO**	**MgO**	**CaO**	**Na_2O**	**K_2O**	**P_2O_5**	**Cl**	**F**	**Total**
Lipari obsidian	5 µm	75.36	0.07	13.05	1.04	0.55	0.05	0.73	3.50	5.15	0.01	0.34	0.04	99.89
	SD	0.30	0.03	0.03	0.69	0.72	0.01	0.01	0.08	0.06	0.01	0.00	0.06	0.43
	10 µm	74.78	0.08	12.98	1.15	0.42	0.03	0.73	3.85	5.20	0.00	0.34	0.06	99.61
	SD	0.18	0.01	0.13	0.62	0.62	0.02	0.01	0.05	0.06	0.01	0.02	0.03	0.30
	15 µm	73.68	0.06	13.13	1.66	0.02	0.01	0.71	3.82	5.37	0.00	0.35	0.00	98.80
	20 µm	74.22	0.06	12.96	1.19	0.44	0.04	0.72	3.94	5.13	0.00	0.32	0.06	99.08
	SD	0.48	0.02	0.16	0.63	0.64	0.01	0.01	0.06	0.06	0.00	0.02	0.03	0.37
Hunt and Hill (1996)	12 µm	74.35	n.d.	12.87	1.51	0.07	0.05	0.74	3.93	5.11	n.d.	n.d.	0.35	98.98